BULGARIAN ACADEMY OF SCIENCES
INSTITUTE OF INFORMATION AND COMMUNICATION TECHNOLOGIES

GABRIELA VIKTOROVA KOTSEVA

MECHANICAL AND TRIBOLOGICAL STUDIES OF POLYMERS AND COMPOSITES PRODUCED BY 3D PRINTING

ABSTRACT OF PhD THESIS

Supervisor:

Prof. Dr. Nikolay Ivanov Stoimenov

Sofa, 2025

Content

Introduction

A primary concern of modern industry and society is the development and continuous improvement of energy-efficient technologies. For society as a whole, this contributes to the preservation of natural resources and minimizes the negative environmental impact caused by excessive fuel consumption. For industry, it ensures compliance with consumer and regulatory demands, thereby maintaining competitiveness. The science of tribology lies at the heart of this pursuit of energy-efficient technologies on many different levels.

Tribology plays a role in the development of energy-efficient technologies at various levels—for example, in manufacturing, by enabling components to operate with long service life and low friction, and in the creation of practical, innovative, energy-saving engines and transmissions. Five specific areas are considered in which tribology faces challenges posed by the development of energy efficiency. These range from reducing friction in components and the resulting difficulties involving very thin hydrodynamic films, to tribological issues inherent in the development of high-temperature adiabatic engines. In all these areas, as well as in many others, it is concluded that tribology plays a key role in the implementation of energy-efficient technologies.

The present dissertation is structured as follows:

Chapter 1 provides an overview and analysis of tribology as a science and engineering discipline. The historical development of tribology worldwide and in Bulgaria is traced, along with its industrial significance. Fundamental principles and applications are presented, together with classical theories of friction and methods for determining the friction force. Mechanical properties (hardness, deformation, fatigue), chemical properties (adsorption, boundary lubrication, surface films), and physical properties (adhesion, thermal conductivity, etc.) are reviewed. Various forms of wear are analyzed, as well as 3D printing technologies, materials (polymers, composites), and their properties.

Chapter 2 describes existing methods for tribological studies of polymers and composites, along with various types of experimental devices. Instruments for measuring microhardness, wear, and friction under different operating conditions are presented, as well as specific testing methodologies. Modern 3D printing techniques and their role in producing test components are also examined.

Chapter 3 outlines methodologies for conducting research on the physico-mechanical and tribological properties of 3D-printed polymers and composites. Procedures for analyzing microhardness, wear, and friction (sliding, rolling, restitution) are defined. Methodologies for using simulation software (EDEM), which enables process modeling, are also included.

Chapter 4 presents experimental results from studies on 3D-printed materials, including composites. Coefficients of restitution and simulation results obtained with EDEM software are analyzed. Comparisons and generalizations are made regarding the influence of different materials and parameters on their tribological characteristics.

Chapter 5 discusses future directions for the development of the dissertation. The obtained experimental results allow for expanding the research aimed at improving 3D-printed components. Another possible aspect is the extension of tribological studies in the field of 3D printing and its applications. Accurate determination of key properties enables the creation of more precise simulation models.

Aim and Objectives of the Dissertation

Based on the review and comparative analysis of the current state of achievements in the field of tribology, the aim of the present dissertation is formulated.

AIM:

The aim of this dissertation is to obtain new knowledge regarding the parameters and characteristics of polymers and composites produced by 3D printing through the investigation and determination of their mechanical and tribological properties. The work seeks to optimize technological processes and develop new approaches for designing functional polymer and composite materials manufactured via additive technologies. Additionally, it aims to improve input data for simulation processes, which would lead to more accurate results.

OBJECTIVES:

To achieve the stated aim, the following objectives must be addressed:

1. To conduct a review and analysis of tribological processes, technologies, and devices for producing polymers and composites, as well as methods for studying the physico-mechanical and tribological properties of polymers obtained through 3D printing.
2. To develop principles and approaches for investigating the physico-mechanical and tribological properties of 3D-printed polymers.
3. To analyze the microhardness and wear characteristics of 3D-printed materials.
4. To analyze sliding friction, rolling friction, and the coefficient of restitution.
5. To perform simulation studies of 3D-printed samples using EDEM Software.
6. To carry out simulation modeling of the coefficient of restitution.
7. To propose a comprehensive approach for characterizing the 3D printers used in the study.
8. To conduct and analyze experimental investigations.

Approbation of the Results

The results included in the dissertation have been presented at international conferences both in Bulgaria and abroad.
Part of the findings has been reported at the following conferences:

List of Publications Related to the Dissertation
At International Conferences Abroad

1. Kotseva, G. & Stoimenov, N. (2025). *Overview of tribology as an interdisciplinary science*. In: 19th International Conference on Tribology – SERBIATRIB '25. Kragujevac: Faculty of Engineering, University of Kragujevac. ISBN 978-86-6335-128-8.
2. Stoimenov, N., Gyoshev, S. & Kotseva, G. (2025). *A Study of the Hardness of 3D-Printed Materials for Blind Applications*. 3rd International Conference on Computers in Natural Sciences, Biomedicine and Engineering (COMCONF), accepted for publication.
3. Kotseva, G., Stoimenov, N., Gyoshev, S., Georgieva, V. (2025). *Tribological Processes in TPU and HIPS 3D Printing Materials*. 18th International Conference on Control, Automation, Robotics and Vision (ICARCV 2024), published by IEEE, pp. 1136–1141.
4. Kotseva, G., Stoimenov, N., Kandeva, M. (2023). *Tribological processes in the material for 3D printing filament HIPS*. 12th International Conference on Mechanical Technologies and Structural Materials (MTSM 2023), Croatian Society for Mechanical Technologies, Croatia, ISSN 1847-7917, pp. 137–144.

At International Conferences in Bulgaria

1. Kotseva, G., Stoimenov, N., Klochkov, L. (2023). *Tribological Studies of 3D Printed Filaments: An Overview*. XXXII International Scientific and Technical Conference ADP – 2023, Sozopol, Bulgaria. Publishing House of TU-Sofia, Department "Automation of Discrete Production Engineering", ISSN 2682-9584, pp. 150–154.
2. Kotseva, G., Georgieva, V., Gyoshev, S. (2023). *Investigation of Tribological Parameters of 3D Printed Samples*. International Scientific Journal Machines. Technologies. Materials, 19(8), Scientific and Technical Union of Mechanical Engineering, ISSN (Print) 2535-0153, ISSN (Online) 2535-0161, pp. 255–259.
3. Stoimenov, N., Kotseva, G., Georgieva, V. (2025). *Classification of 3D Print Technologies*. 34th International Scientific and Technical Conference Automation of Discrete Production Engineering 2025, ISBN 978-619-7667-74-5, DOI: 10.53656/adpe-2025, Publisher: Az-buki National Publishing House, pp. 40–53.

Chapter 1

Literature Review and Analysis. Fundamental Principles and Applications of Tribology. Technologies, Devices, and Methods for Studying 3D-Printed Polymers

1.1. Engineering Tribology. Tribology as a Science

Tribology is an interdisciplinary field that studies friction, wear, and lubrication of contacting surfaces in relative motion. It plays a crucial role in engineering—from the automotive and aerospace industries to mechanical engineering—by contributing to extended service life and reduced energy losses of mechanical systems [1–3].

The advancement of tribology supports the development of new materials and technologies with improved characteristics, and losses caused by friction and wear may reach 5–7% of a nation's GDP, which highlights its economic and technological significance [4].

1.1.1. Historical Development of Tribology

Tribology examines friction, lubrication, and wear of interacting surfaces. The term originates from the Greek word *tribos*, meaning "rubbing" or "friction" [1–3].

Friction has been applied since ancient times—from fire making and tool crafting to the use of natural bitumen as a lubricant. Archaeological evidence from Egypt shows an early use of bearings in potter's wheels (Fig. 1.1), as well as the application of liquid lubricants during the transportation of massive stone blocks (Fig. 1.2).

Fig. 1.1. *Wooden bearing for stone wheels, Ancient Egypt.*

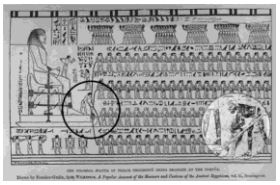

Fig. 1.2. *Transporting an Egyptian statue, El Bersheh, around 1900 BCE.*

1.1.2. Brief Overview of Tribology in Bulgaria

Targeted research in the field of tribology in Bulgaria began in 1963 with the establishment of the Laboratory of "Contact Mechanics" at the Technical University of Sofia, founded by Prof. Dr. Georgi Danov [5]. In 1974, the laboratory was reorganized into the "Tribology Laboratory" under the leadership of Prof. Nyagol Manolov [6], and later developed into a National Coordination Centre. Since 1984, Bulgaria has been a regular member of the International Council of Tribology.

In 1993, the Society of Tribologists in Bulgaria (STB) and the Balkan Tribological Association (BTA) were established, with Prof. DSc N. Manolov as the first chairman. The BTA, which includes six Balkan countries, organizes regular scientific conferences. In 2008, the VI Anniversary Conference "Balkantrib'08" was held in Sozopol (Assenova, Kandeva, 2008) [7], featuring around 130 papers across nine scientific sections.

Today, the Tribology Laboratory continues its active research, educational, and applied activities. A modern concept for the development of tribology has been formulated (Manolov et al., 2007) [8], included in the national scientific classification under No. 01.02.02 (State Gazette, Issue 34/1990) [9]. An annual seminar "Tribology and Interdisciplinarity" is held, and a National Expert Council on

Tribology operates within INGA. The journal *Kontakt*, with Editor-in-Chief Prof. DSc N. Manolov, presents new scientific contributions in the field of contact interactions [10]. Tribological research groups also function within the Bulgarian Academy of Sciences and several universities across the country.

1.1.3. Development of Tribology Worldwide

Tribology is well developed in leading industrial countries, where it plays a key role in optimizing mechanical systems and enabling technological innovation.

In the United States, extensive research is carried out in universities, national laboratories, and industry, particularly in the automotive, aerospace, and energy sectors, which widely implement tribological technologies [11].

Germany is a global leader due to its strong automotive and mechanical engineering industries, supported by advanced research institutions [12].

In Japan, tribology is integral to the development of high-performance components in the automotive, electronics, and robotics industries [13].

The United Kingdom has long-standing traditions in tribology, and the Institute of Tribology at the University of Leeds is internationally recognized as one of the leading scientific centres [11].

In recent decades, China has significantly increased its research activity, focusing on improving manufacturing technologies and expanding industrial applications [14].

These countries invest substantial resources in tribology, resulting in major technological advances and increased efficiency across multiple sectors.

1.1.4. Industrial and Economic Importance of Tribology

The industrial revolutions have introduced new tribological challenges related to friction, wear, and lubrication of interacting surfaces. The main objective of tribology is to reduce energy and material losses through optimized lubrication, surface modification, and the development of improved materials [15,16].

Approximately 23% of global energy consumption is directly related to tribological contacts and friction losses [17], highlighting the significant economic potential of tribological improvements.

For example, in the United States, optimizing the lubrication of about 3 million worm gears (7.5 kW each) increases their efficiency by 5%, saving 9.8 billion kWh of energy and about 0.6 billion USD. Globally, modern tribological technologies can reduce energy losses by 40% over 15 years and by 18% over 8 years, equivalent to about 1.4% of global GDP [18].

In the United Kingdom, modern tribological solutions can reduce wear-related maintenance costs by up to 95% within a 10-year period, consistent with the predictions of the Jost Report [19].

1.2. Fundamental Principles and Applications of Tribology

Although the term *tribology* may be unfamiliar to non-specialists, its principles are present in nearly all everyday and industrial processes. From bearing operation and automotive components to the behaviour of biological tissues, tribological phenomena determine efficiency, reliability, and durability in engineering systems and natural structures.

Figure 1.4 presents a classification scheme summarizing the significance of tribology, its fundamental principles, applications, general theories, classical methods, and the characteristic forces

and coefficients involved in contact interactions. The figure also outlines the industrial and economic relevance of tribology and its importance in modern technological development.

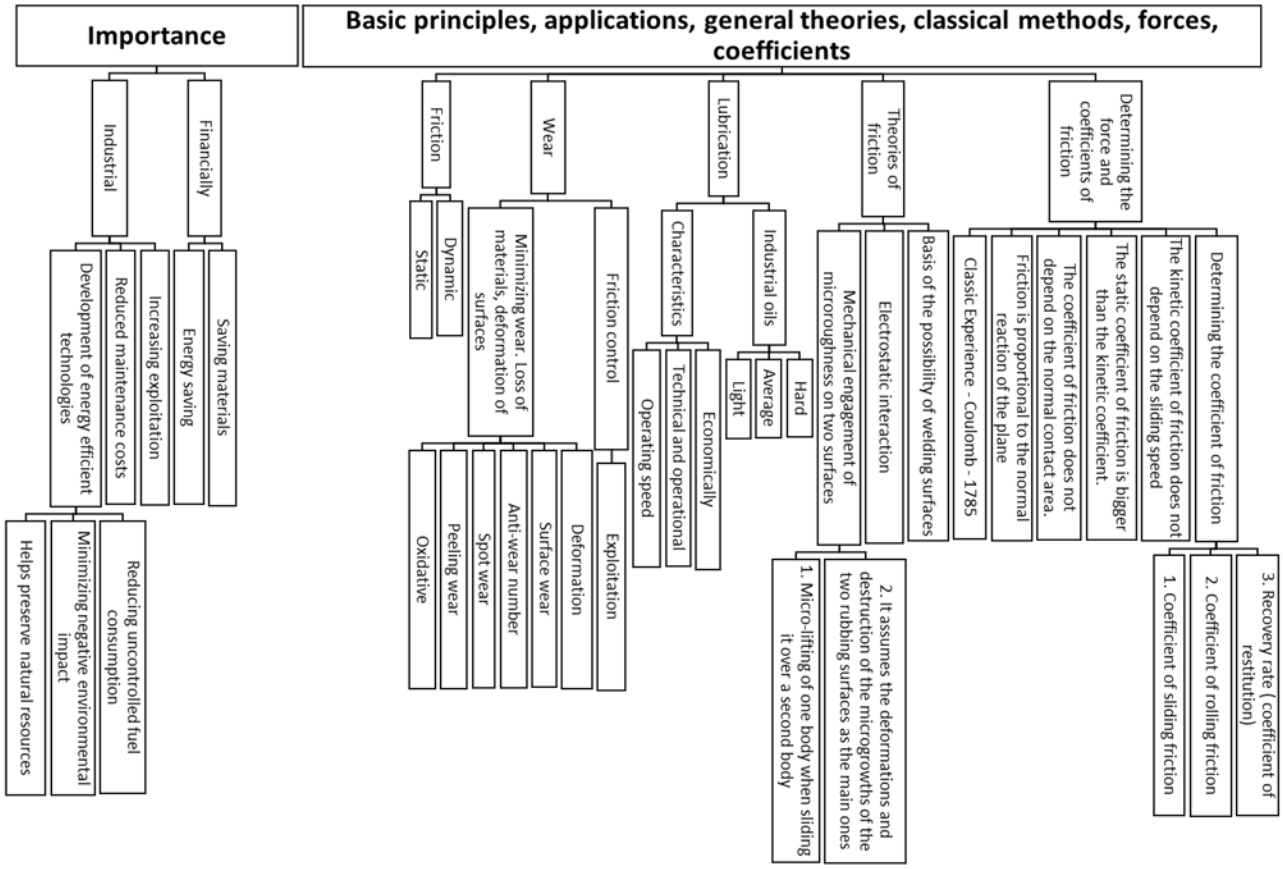

***Fig. 1.4**. Diagram – Classification of the Fundamental Principles of Tribology*

1.2.1. Introduction to Tribology

Currently, tribology, a relatively new scientific field, is defined in many dictionaries as *"the science of interacting surfaces in relative motion"* or *"the study of friction, wear, and lubrication, as well as the design of bearings"* [20]. Figure 1.5 illustrates the tribology triangle.

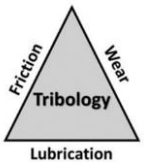

***Fig. 1.5.** The Tribology Triangle*

1. **Friction** – Friction is a natural phenomenon with an important role in everyday life. In tribology, however, it is primarily considered as a source of wear and energy loss. Two regimes of friction are distinguished: static and kinetic (dynamic). In both cases, friction represents a force acting opposite to the direction of motion or potential motion between surfaces [21].
2. **Wear** – Wear is a fundamental process involving the loss of material or surface deformation, which can lead to the failure of mechanical components. In tribology, it is viewed as the gradual removal of material due to mechanical and/or chemical interactions between surfaces [22], and is defined as the progressive loss of substance during relative motion [23–25].
3. **Lubrication** – Lubrication is a key method for reducing friction and controlling wear. The term derives from the Latin *lubricatus* ("to make slippery") and refers to a substance that modifies the interaction between contacting surfaces. Lubricants may be liquids, greases, solid lubricants, or

gases. Their primary function is to reduce friction, wear, and thermal stress; without them, direct contact occurs, increasing the risk of damage [21].

- Lubricant Types – Lubricants are classified as liquids, greases, solids, and gases.
- Oil Characteristics – Industrial lubricating oils are available in various types, and proper selection is critical for specific applications. Depending on their origin, oils may be mineral, synthetic, or blended.

1.2.2. Parameters Characterizing Surface Interactions

To analyze processes related to friction, various theories have been developed that reflect the characteristics of different materials, surface roughness, and applied pressure. These include: the theory of mechanical interlocking, the theory of electrostatic interaction, and the theory based on the potential for surface "welding."

Tables 1.1 and 1.2 are taken from *Coefficients of Friction* in *Theoretical Mechanics*, Bozhidar Toshev, Technika, 1973 [26].

Table 1.1. Interaction of Tribo-Pairs under Sliding

Двойка (при плъзгане)	При покой	При движение
Стомана – Чугун	0.15	0.1
Стомана – Лед	0.017	0.014
Стомана – Дърво	0.55	0.4
Дърво – Дърво	0.65	0.35
Дърво – Камък	0.7	0.3
Кожа – Метал	0.6	0.25

Table 1.2. Interaction of Tribo-Pairs under Rolling

Двойка (при търкаляне)	[mm]
Вагонно колело – Релса	0.6
Дървено колело – Дърво	15.0
Автомобилна гума – Асфалт	45.0
Автомобилна гума – Паваж	25.0

1.2.3. Existing Standard Methods for Testing Friction, Wear, Adhesion, and Restitution

Standardized methods for testing the main mechanical parameters—such as sliding friction, rolling friction, coefficient of restitution—as well as additional characteristics like adhesion, wear (wear coefficient), and abrasion, according to internationally recognized standards, are presented in Tables 1.3–1.6:

Table 1.3. *Sliding Friction*

Standard	Application Area	Notes
ISO 8295:1995	Static and kinetic friction coefficient for plastic films and sheets (≤0.5 mm)	Mainly for quality control
ASTM D1894-24	Plastic films	American counterpart; results not fully comparable with ISO 8295
ISO 6601:2002	General standard for sliding friction and wear testing	Defines conditions such as load, speed, and contact parameters
ASTM E1911-19	Dynamic Friction Tester	Allows evaluation of friction as a function of speed; applicable in lab and field conditions

Table 1.4. Rolling Friction

Standard	Application Area	Notes
ISO 18164:2005	Rolling resistance of new pneumatic tires (cars, buses, motorcycles)	Measurement under free-rolling and controlled conditions
ISO 18164:2005/DAM 1	Deceleration approach	Uses time–distance dependency to calculate resistance
ISO 28580:2018	Rolling resistance of road tires	Modern method, potentially replacing ISO 18164

Table 1.5. Coefficient of Restitution (COR)

Standard	Application Area
ASTM F1887	Vertical drop of a ball onto a hard surface
ISO 10545-5	COR measurement for ceramic tiles
ASTM C203	Impact behavior and restitution of low-density materials, including polymer composites

1.3. Mechanical Properties

The classification of mechanical properties and the chemistry of tribo-surfaces is presented in Fig. 1.12. The mechanical section includes hardness (indentation and scratch), deformation (elastic and plastic, including slip and failure), fatigue, and durability as key indicators of long-term performance under load.

The chemical section considers processes such as adsorption, boundary lubrication formation, and surface film development, as well as diffusion. Adhesion and corrosion are also included, along with specific phenomena in microelectromechanical systems (MEMS), where surface interactions are critically important.

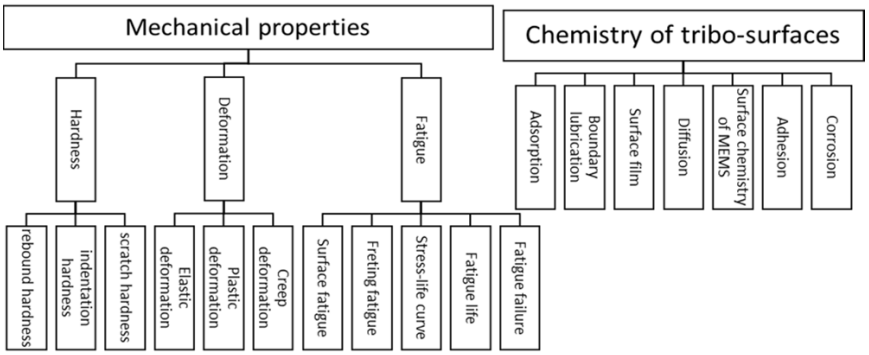

Fig. 1.12. *Diagram – Classification of Components in Tribology: Mechanical Properties and Chemistry of Tribo-Surfaces*

1.3.1. Hardness

Hardness describes a material's ability to resist permanent deformation or penetration, with higher hardness indicating greater resistance to applied loads. The main types of hardness are: indentation hardness, scratch hardness, and rebound hardness.

1.3.2. Deformation

1. **Elastic Deformation**
   This is an instantaneous and recoverable change in shape or size that occurs only under applied normal stress and disappears once the load is removed [27]. Elastic deformation is determined by the Young's modulus (E). Exceeding a certain threshold leads to **plastic**, i.e., permanent, deformation [28].

2. **Plastic Deformation**
   In a stress–strain curve, when a material specimen is subjected to increasing stress beyond the yield point (Y), it no longer returns to its original shape after unloading. Deformation beyond the yield point is time-independent and is referred to as **plastic deformation** [29].
3. **Creep Deformation**
   Creep is the gradual change in the shape of a material under constant stress and elevated temperature, potentially leading to failure. Creep strength depends on both stress and time, and under cyclic loading, fatigue accelerates due to the interaction between creep and fatigue [30, 31]. The typical creep curve includes three stages:
   - Primary (transient) stage: elastic and partially plastic deformation
   - Secondary (steady-state) stage: gradual nearly constant increase in deformation
   - Tertiary stage: accelerated deformation leading to failure

1.3.3. Fatigue

Fatigue is a critical factor in engineering design, responsible for over 80% of mechanical failures [29]. As early as the 1800s, it was observed that cyclic loads caused cracking in bridges and railway structures.

1. **Fatigue Failure** – Under cyclic loading, microcracks can initiate on surfaces, gradually grow to a critical size, and lead to failure.
2. **Fatigue Life** – Typically considered in two stages: (1) crack initiation, and (2) crack propagation [29].

1.4. Chemistry of Tribo-Surfaces

The chemistry of tribo-surfaces examines processes occurring at the contact interface between surfaces and their interactions with the environment (liquids, gases, vacuum). Surface phenomena include **adsorption**, **diffusion**, **adhesion**, surface forces, and chemical reactions. Since surface atoms have different chemical states compared to bulk atoms, they are more reactive, and **adsorption** is often a key step in these processes [32, 33].

1.4.1. Adsorption

Adsorption is the attachment of atoms, ions, or molecules to a material surface (adsorbent), differing from absorption, where particles penetrate the bulk. Two main types are distinguished:

- **Physisorption** – via weak Van der Waals forces
- **Chemisorption** – via chemical bonds between adsorbate and adsorbent

In tribology, particularly under boundary lubrication, adsorption and subsequent surface reactions play a key role in the effectiveness of lubricants and additives [34].

1.4.2. Boundary Lubrication

Boundary lubrication occurs under extreme conditions—high loads and/or low sliding speeds—where the lubricating film is very thin (a few molecular layers). Its formation is primarily based on adsorption, and tribochemical reactions determine the film's composition and protective properties on the tribo-surfaces [35]. According to monolayer theory, adsorbed and oriented molecules prevent direct contact between surfaces and reduce friction due to their low shear strength, as illustrated in Fig. 1.15 [36]

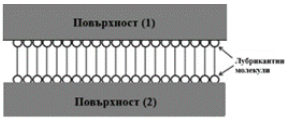

***Fig. 1.15**. Illustration of boundary lubrication showing a monolayer of lubricant molecules adsorbed and oriented on the contacting surfaces.*

1.4.3. Surface Film

Most metals and alloys form natural oxide films in air, and under various conditions, sulfide, nitride, or chloride coatings may also form [25]. Their thickness is typically on the nanoscale and depends on the chemical reactivity of the metal; for example, the oxide film on stainless steel is only a few nanometers thick [37]. These films influence tribological behavior according to their chemical and mechanical properties: soft, adherent films act as lubricating layers that separate contacting surfaces, while hard and brittle films crack easily and are less effective.

1.4.4. Diffusion

In chemistry, diffusion refers to the movement of fluid molecules within solids, typically porous materials. In tribology, **diffusion treatment** (or the Diffusion Annealing Process, DAP) refers to the modification of a surface by introducing interstitial or substitutional atoms from an external source [38–40]. Annealing is often used to regulate the microstructure and properties of materials by heating above the recrystallization temperature, holding, and slow cooling.

1.4.5. Surface Chemistry of MEMS

Surface properties of microelectromechanical systems (MEMS) are critical due to their extremely high surface-to-volume ratio. It is well established that controlling surface forces—particularly adhesion between contacting surfaces—is a key challenge in the operation and maintenance of MEMS devices [41–44].

1.5. Physical Properties

In tribology, the physical properties of materials and surfaces determine friction, wear, and lubrication. They affect contacts at the atomic, micro-, and macro-scale. Key parameters include adhesion, roughness, hardness, thermal and electrical conductivity, viscosity, and others, which control the effectiveness of lubricating films and the accuracy of contact mechanics.

Adhesion is described through normal and adhesive forces, the coefficient of cohesion, surface energy, environmental conditions, oxidation, friction, and material transfer. Wettability is characterized by surface tension and the contact angle, considering complete and partial wetting and the dynamics of the process under different surface states.

Figure 1.16 systematizes these properties and their interrelationships through formulas and dependencies that characterize material behavior under contact.

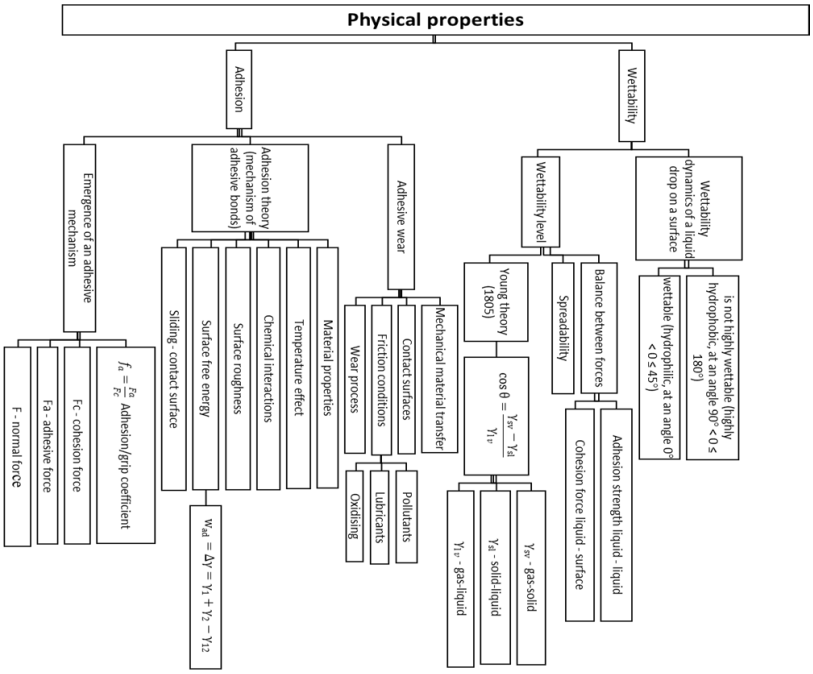

***Fig. 1.16**. Diagram – Classification of Physical Properties in Tribology*

1.6. Forms of Wear

Wear by abrasion, erosion, and cavitation occurs due to interactions between solid particles or fluids and the material surface.

These processes are among the most aggressive wear mechanisms, and differences in their micromechanisms determine the selection of materials and methods for improving wear resistance [45].

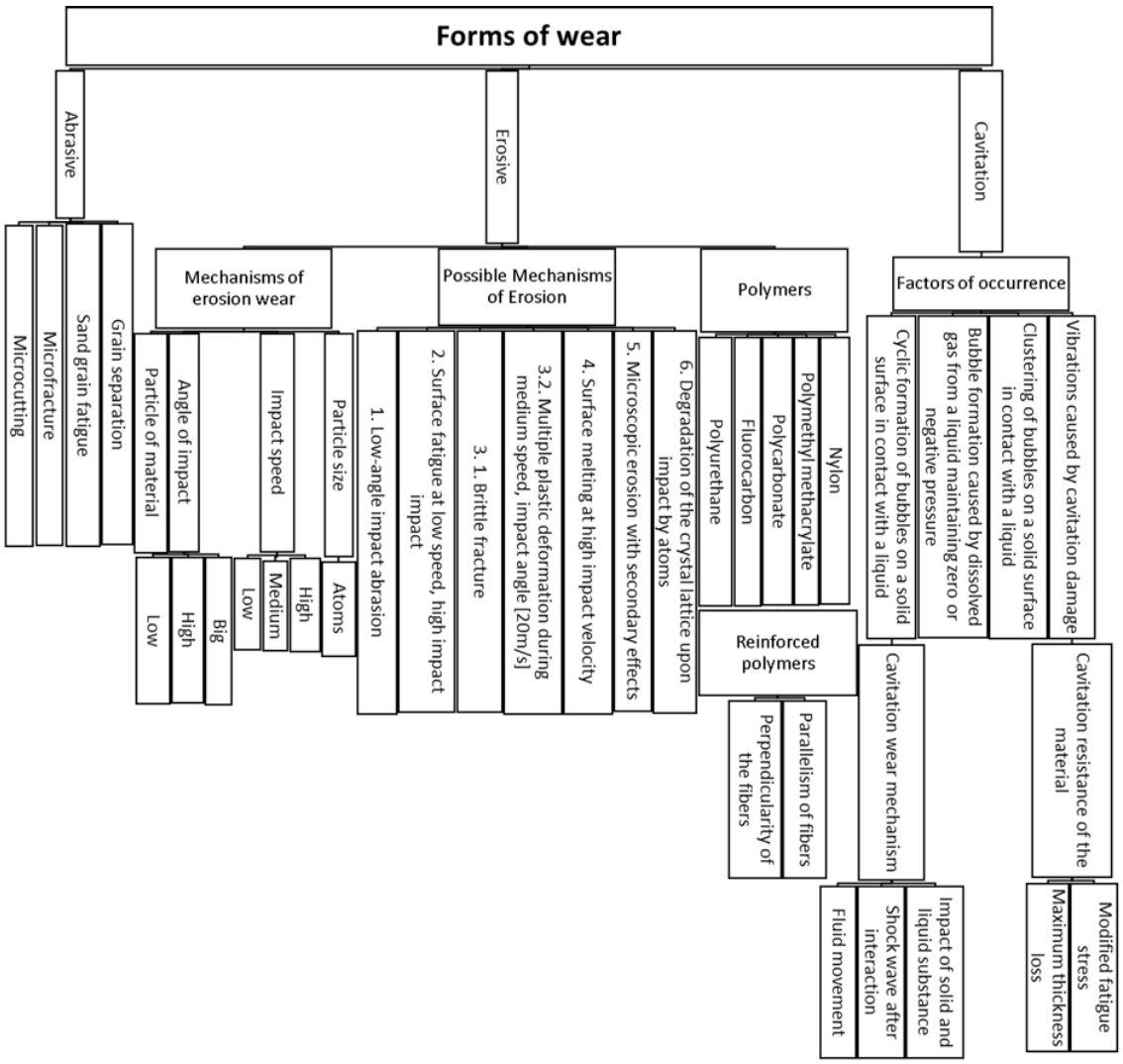

Fig. 1.19. *Diagram – Classification of Wear Forms in Tribology*

1.6.1. Abrasive Wear

Abrasive wear occurs whenever a hard object is pressed against particles of a material that have equal or greater hardness. A common example is the wear of excavator blades. The degree of abrasive wear is often much higher than expected. Any material, even if most of it is very soft, can cause abrasive wear. For instance, an organic material such as sugarcane is associated with abrasive wear on cane cutters and shredders due to the small fraction of silicon dioxide present in the plant fibers [45].

1.6.2. Erosive Wear

Erosive wear is caused by the impact of solid particles or liquids on a surface. It occurs in a wide variety of machinery; typical examples include damage to gas turbine blades when an aircraft flies through dust clouds, and wear of pump impellers in systems handling mineral suspensions. Similar to other forms of wear, mechanical strength alone does not guarantee wear resistance, and detailed

material characterization is required to minimize wear. Known mechanisms of erosive wear are illustrated in Fig. 1.21.

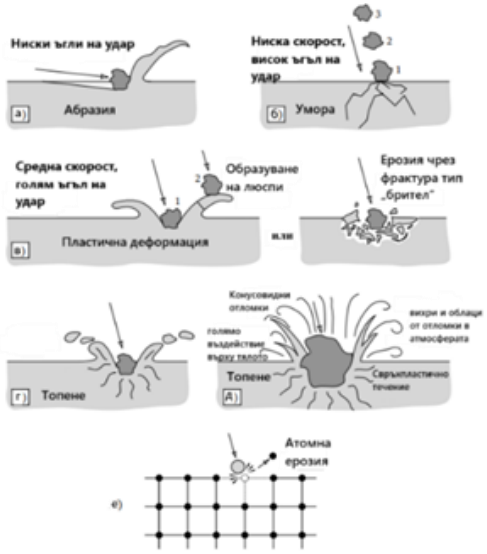

Fig. 1.21. *Possible Erosion Mechanisms: a) Abrasion at low impact angles; b) Surface fatigue from low-speed, high-angle impacts; c) Brittle fracture or repeated plastic deformation from medium-speed, high-angle impacts; d) Surface melting at high impact velocities; e) Macroscopic erosion with secondary effects; f) Degradation of the crystal lattice from atomic impacts.*

1.6.3. Cavitation Wear

Cavitation wear is known to damage equipment such as impellers or turbine blades operating in wet steam, as well as valve seats. The wear progresses through the formation of a series of pits or cavities on the surface exposed to cavitation. This process can lead to the complete destruction of the machine component. The operation of equipment, for example an impeller, is often limited by severe vibrations caused by cavitation damage.

1.7. Conclusion

From the analysis of tribology as an interdisciplinary science, it is evident that it plays a key role in modern industry and the economy. By optimizing friction, wear, and lubrication, tribology contributes to the improvement of manufacturing processes, sustainable resource usage, and the reduction of negative environmental impacts. Investments in tribological research and technologies provide long-term benefits, supporting more environmentally friendly and cost-effective solutions.

The classification of tribology according to fundamental principles, applications, mechanical and physical properties, chemical interactions of tribo-surfaces, and forms of wear provides an essential foundation for optimizing industrial systems. Studying forces and friction coefficients enables increased efficiency, reduced maintenance costs, and the development of innovative solutions.

Chapter 2

Tribological Research Technology: Devices and Experimental Equipment

Experimental tribological research consists of a set of methods, devices, and procedures used to evaluate the primary parameters of friction, wear, and lubrication. Such research is essential not only for the development of new materials and surface coatings but also for optimizing existing engineering solutions in mechanical engineering, energy, the automotive industry, and biomedicine.

2.1. Existing Methods and Types of Tribological Research on Polymers and Composites

Tribological studies investigate friction, wear, and lubrication between surfaces to assess material durability and optimize systems. They are conducted in laboratories using tribometers and specialized setups that control load, speed, and environmental conditions.

2.2. Devices for Testing Microhardness of Polymer Materials

The hardness of plastics indicates their resistance to indentation and quantitatively reflects their softness or stiffness. Although it does not directly correspond to other mechanical properties, hardness is an important indicator for quality control. The most commonly used methods are Shore and Rockwell, with the Shore method being widely applied in the rubber and plastics industries. Other popular methods include Vickers, Knoop, Brinell, and Mohs, with the choice depending on the specific material application [46].

Devices used for testing the hardness of polymers and composites in this dissertation include:

- **Instruction Manual Digital Shore Hardness Tester SAUTER HD** – The digital Shore hardness tester SAUTER HD (Fig. 2.3) is an electronic instrument for determining the surface hardness of elastomers, rubber, plastics, soft polymers, and other non-rigid materials. It measures the depth of penetration of an indenter under a given force, displaying the result on a digital screen in Shore units (A or D depending on the model).

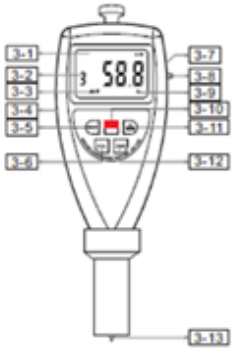

***Fig. 2.3**. Front Panel Description: 3-1 Display; 3-2 Number of measurements in average mode; 3-3 Average value indicator; 3-4 RS-232 interface; 3-5 Max HOLD button; 3-6 CAL button; 3-7 Battery cover; 3-8 Wrist strap ring; 3-9 Average value status; 3-10 Power button; 3-11 N/Average button; 3-12 Reset button; 3-13 Sensor (indenter)*

- **Hardness Tester EBP BRV-187.5T** – For hardness testing, a digital universal hardness tester EBP BRV-187.5T was used, shown in Fig. 2.4. It is capable of performing tests according to Brinell, Rockwell, and Vickers methods. The device operates with a testing force range from 5 kgf to 187.5 kgf, applying a closed-loop system with a high-precision load cell, which ensures accurate load application without the need for physical weights.

Fig. 2.4 *Hardness Tester EBP BRV-187.5T [47]*

The device is operated and the results are recorded via an 8-inch touchscreen. The optical system includes a microscope with 2.5× and 5× objectives (optional: 10×, 20×) and a 15× eyepiece, providing up to 75× magnification and a minimum resolution of 0.1 μm. The tester complies with ISO 6508, ASTM E-18, ISO 6506, ASTM E10, ISO 6507, and ASTM E92 standards, allowing measurements in the ranges of 8–650 HBW, 20–100 HR, and 8–2900 HV.

2.3. Equipment for Measuring the Coefficient of Restitution – High-Speed Camera NAC MEMRECAM HX6

In the study to determine the parameters of the coefficient of restitution, a high-speed camera and specialized accompanying software are used. This setup enables the measurement of all rebound parameters of a 9 mm diameter sphere dropped onto a 60 × 60 × 10 mm plate, as described in the dissertation. Figure 2.7 shows the high-speed camera NAC MEMRECAM HX6 [48].

Fig. 2.7. *High-Speed Camera NAC MEMRECAM HX6*

The camera is equipped with 32 GB of internal memory, a CMOS sensor with a maximum resolution of 2560×1920 px at 1000 fps, external synchronization, three interchangeable lenses (including a vario lens), temperature calibration, and additional illumination from two 1 kW spotlights. It is controlled via specialized software and supports USB and Ethernet interfaces, remote control, and local playback.

Some of the fields and applications for which the NAC MEMRECAM HX-6 is used include: ballistics and projectile testing; explosive and pyrotechnic tests; material and deformation testing; flow visualization (e.g., PIV – Particle Image Velocimetry); optical synchronization and high-precision time measurements; and segmented recording — the camera can record in two different segments with different settings simultaneously.

2.4. 3D Technologies, Materials, and Printing Devices

Additive manufacturing is a process for creating three-dimensional objects from a digital model by sequentially depositing material layer by layer. With layer thicknesses of 16–180 μm, this technology allows fast and cost-effective production of parts, prototypes, and molds, replacing traditional methods such as turning and casting.

The quality of the part mainly depends on: layer thickness, fill pattern and angle, and printing orientation. By optimizing these parameters, higher accuracy, strength, and a better surface finish of the part are achieved [49, 50].

The most widely used 3D printing processes for plastics are:

- FDM (Fused Deposition Modelling) – extrusion of molten thermoplastic filament layer by layer.
- SLA (Stereolithography) – curing of liquid resin through laser photopolymerization.
- SLS (Selective Laser Sintering) – laser sintering of thermoplastic powder.

The technological processes are schematically presented in Fig. 2.8.

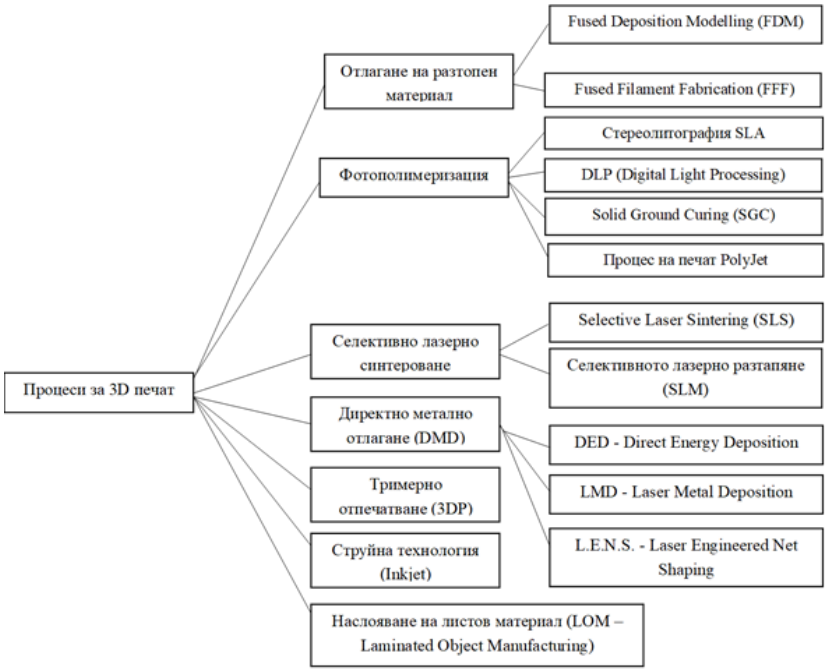

Fig. 2.8. *Diagram of the 3D printing processes*

2.4.1. Deposition of Melted Material (FDM or FFF)

3D printers operating on the Fused Deposition Modelling (FDM) principle melt and extrude a thermoplastic filament, which the nozzle deposits layer by layer in the build area [49,51]. The technology is illustrated in Fig. 2.9.

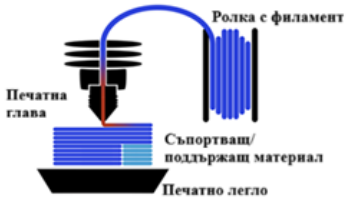

Fig. 2.9. *FDM – Layer-by-Layer Printing Diagram*

2.4.2. Photopolymerization – Stereolithography (SLA), DLP (Digital Light Processing), and PolyJet Printing Process

Stereolithography (SLA) is a high-precision 3D printing technology in which a UV laser cures a photopolymer resin layer by layer through photopolymerization. The 3D models are prepared using CAD and converted into STL/OBJ files. The resins contain monomers, oligomers, and photo-initiators, which form a cross-linked structure when exposed to UV light [50-51].

The layer thickness is approximately 100 μm, with a curing time of 3–15 seconds. After printing, the parts are cleaned and subjected to additional UV curing [52]. SLA is used in medicine, tissue engineering, and industrial prototyping [53, 54].

Limitations include the use of epoxy/acrylate resins with a high carbon footprint and their difficult recyclability, which has driven the development of biodegradable alternatives [52–55].

PolyJet – PolyJet is a high-precision 3D photopolymerization technology with a resolution of up to 0.014 mm, allowing the combination of different materials [56]. It is used to produce smooth and detailed prototypes, medical models, and functional parts. The process is schematically shown in Figure 2.10.

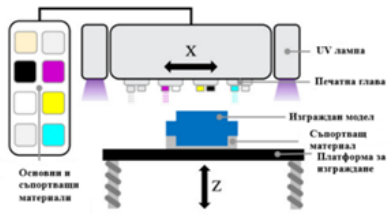

Fig. 2.10. *Illustration of 3D printing using PolyJet technology*

2.4.3. Selective Laser Processes

Selective Laser Sintering (SLS) is a 3D printing technology in which a laser sinters a powdered material—most commonly nylon—layer by layer according to a 3D model [57]. Each powder layer is spread over a heated platform and sintered in the designated areas, with the process repeating until the entire object is built [57, 58].Figure 2.11 illustrates the general workflow of the selective laser sintering process: 1 – Model being built;2 – Powdered material; 3 – Powder feed hoppers; 4 – Roller for even distribution of the powder; 5 – Laser beam; 6 – Build chamber; 7 – Pistons moving along the Z-axis; 8 – Laser source; 9 – Lenses; 10 – Mirror guiding the beam along X and Y axes.

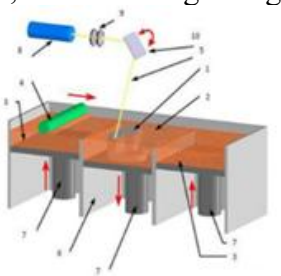

Fig. 2.11. *General view of the technological process in Selective Laser Sintering (SLS)*

2.4.4. Direct Metal Deposition (DMD)

Direct Metal Deposition (DMD), also known as Direct Metal Deposition, is an additive manufacturing technology used for fabricating and repairing metal components by precisely feeding metal powder or wire into a melt pool created by a high-energy laser or electron beam source [59]. This technique includes several variants under the umbrella of Direct Energy Deposition (DED), such as Laser Metal Deposition (LMD), Laser Engineered Net Shaping (LENS), and others [60]. Figure 2.13 presents a general overview of the DMD technological process.

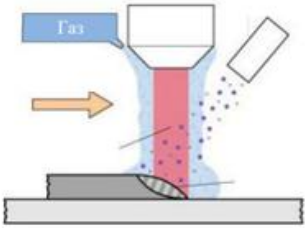

Fig. 2.13. *General view of the technological process in Direct Metal Deposition (DMD)*

2.4.5. Three-Dimensional Printing (3DP)

Three-dimensional printing (3DP) is an additive manufacturing technology developed at the Massachusetts Institute of Technology (MIT) in the USA in the early 1990s [61]. The method is based on the principle of inkjet binding, where a binding agent is jetted onto layers of powder material through a nozzle, similar to inkjet printers. Once the binder is applied, the particles bond together, while the unbound material remains as a filler and can be reused [62].

Figure 2.14 shows the technological scheme of the process. After the model is built, it is removed from the powder bed, cleaned of excess powder, and sintered in a furnace. This improves the mechanical properties of the part.

This method does not require support structures, as the unbound powder itself serves that function.

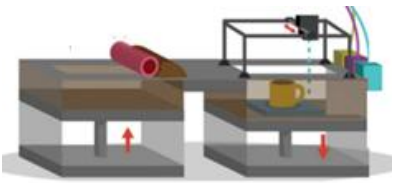

Fig. 2.14 *Technological scheme of the 3DP process*

2.4.6. Inkjet Technology

In this method, an extruding head with two nozzles is used—one for the main material and one for the support material [63]. The main material, often a wax-like polymer, is heated to a liquid state and deposited as fine droplets onto the substrate, where it immediately solidifies. The support material is deposited in the same way. Each layer is milled to the desired thickness, after which the build platform is lowered by the layer height, and the process repeats until the object is complete.

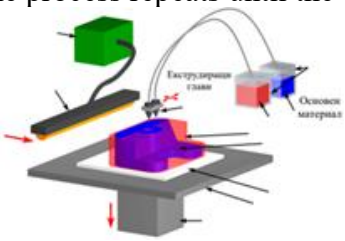

Fig. 2.15 *Technological scheme of the inkjet (3D printing) process*

2.4.7. Laminated Object Manufacturing (LOM)

The Laminated Object Manufacturing (LOM) method involves the sequential layering of sheet materials (e.g., paper) using a bonding agent. In this process, each layer is cut and shaped with a laser beam. The thickness of each layer depends on the thickness of the sheet material used. In addition to cutting the layer contours, the laser beam slices the excess material into square shapes [64]. The technological scheme of the LOM process is shown in Figure 2.16.

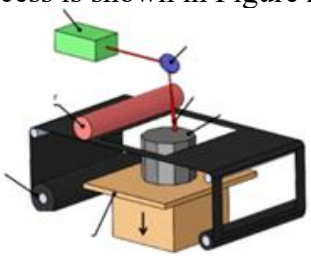

Fig. 2.16 *Technological scheme of the LOM process [152]*

2.4.8. 3D Technologies Used in the Research

In this dissertation, the following 3D printing technologies were used:

- ***3D printers with FDM technology:*** TEVO Tornado (Fig. 2.17); Ultimaker S5 (Fig. 2.18); Bambu Lab P1S (Fig. 2.19).

Fig. 2.17 *TEVO Tornado*

Fig. 2.18 *Ultimaker S5*

Fig. 2.19 *Bambu Lab P1S*

Table 2.1 *presents the specifications of the printers used in this study.*

Printer	TEVO Tornado	Ultimaker S5	Bambu Lab P1S
Overall dimensions	560 × 600 × 620 mm	W 495 × D 585 × H 780 mm	389 × 389 × 458 mm
Number of extruders	1	2	1
Print bed size	300 × 300 × 400 mm	330 × 240 × 300 mm	256 × 256 × 256 mm
Maximum print area	300 × 300 × 400 mm	330 × 240 × 300 mm	256 × 256 × 256 mm
Maximum print speed	150 mm/sec	< 24 mm³/s (build speed)	500 mm/sec
Layer resolution	50 μm (0.05 mm)	0.25 mm nozzle: 60–150 μm; 0.4 mm: 20–200 μm; 0.6 mm: 20–300 μm; 0.8 mm: 20–600 μm	0.08–0.28 mm
Filament diameter	1.75 mm	2.85 mm	1.75 mm
Nozzle diameter	0.4 mm	0.25, 0.4, 0.6, 0.8 mm	0.4 mm (standard), options 0.2 / 0.6 / 0.8 mm
Max extruder temperature	260 °C	180–280 °C	300 °C
Heated bed temperature	60–110 °C	20–140 °C	100 °C
Connectivity	TF card or USB	Wi-Fi (2.4 GHz), Ethernet, USB	microSD, Wi-Fi, Bluetooth
File formats	STL, G-code	UltiMaker Cura: STL, OBJ, X3D, 3MF, BMP, GIF, JPG, PNG; Printable: G, GCODE, GCODE.gz, UFP	G-code (via Bambu Studio and supported slicers)
Compatibility / Materials	Windows, Linux, Mac	PLA, Tough PLA, Nylon, ABS, CPE, CPE+, PC, TPU 95A, PP, PVA, Breakaway, etc.	PLA, PETG, TPU, ABS, ASA, PA (Nylon), PC, PVA, PET; recommended up to 300 °C; carbon/glass filaments not recommended without extruder upgrade

- ***PolyJet Printing Technology*** *– Stratasys Objet260 Connex3*

The 3D printer Stratasys Objet260 Connex3 operates using PolyJet technology, which is distinguished by extremely high precision and the ability to combine different materials and colors in a single printing process [65]. Table 2.2 presents the main parameters and characteristics of the Stratasys Objet260 Connex3 [66-70].

Table 2.2 *Parameters of the 3D printer Stratasys Objet260 Connex3.*

Parameter	Value
Build Volume	255 × 252 × 200 mm
Minimum Top Layer Thickness	Horizontal layers down to ~16 microns (0.016 mm)
Resolution / DPI per Axis	X-axis: 600 dpi; Y-axis: 600 dpi; Z-axis: 1600 dpi
Accuracy	~20–85 μm for features under 50 mm; up to 200 μm for entire models (depending on geometry, orientation, and set parameters)
Materials	- Model photopolymers: Vero series (rigid, transparent, colored), Tango / Agilus (rubber-like), Digital ABS, simulated polypropylene (Rigur, Durus), high-temperature and biocompatible materials - Support material: SUP705 (removed via water jet) and SUP706 (soluble)
Printing Modes	High Quality — minimum layer (~16 μm) Digital Material and High Speed — thicker layers (~30 μm) depending on need for speed or quality
Machine Size / Weight	Printer: ~87 × 120 × 73.5 cm; ~264 kg Material Cabinet: ~33 × 117 × 64 cm; ~76 kg
Power Supply	110–240 VAC, 50–60 Hz (~1.5 kW)
Operating Conditions	Temperature: 18–25 °C; Relative Humidity: 30–70%, non-condensing

The Objet260 Connex3 printer features a print head that allows the simultaneous use of up to three materials in a single object, providing different mechanical properties, transparency, and full-color printing. Model photopolymers (Vero, Tango, Digital ABS) are used for the object, and support material (SUP705/706) is removed after printing.

- **Anycubic Photon M3 Max** – MSLA (Masked Stereolithography Apparatus) printing technology

The 3D printer Anycubic Photon M3 Max uses MSLA technology (Masked Stereolithography Apparatus), also known as LCD-based stereolithography printing [71–75]. Table 2.3 presents the parameters of the 3D printer.

Table 2.3 *Parameters of the Anycubic Photon M3 Max*

Parameter	Value
Printing Technology	LCD / MSLA (Masked Stereolithography)
Screen Size	13.6" monochrome LCD
Screen Resolution	6480 × 3600 pixels (7K)
XY Resolution	46 µm
Z-Axis Accuracy	10 µm
Printing Area Size	300 × 298 × 164 mm (H × D × W)
Print Volume	14.7 liters
Printing Speed	up to 60 mm/h
Lighting System	Anycubic LightTurbo with 84 LED elements
Control Panel	4.3" color touchscreen LCD
Input	USB-A 2.0
Rated Power	120 W
Print Platform	Laser-engraved for better adhesion
Slicing Software	Anycubic Photon Workshop
Additional Features	Smart resin refill, screen protection with anti-scratch film

MSLA technology is particularly suitable for printing high-resolution parts with smooth surfaces using photopolymer resins (UV resins). The Anycubic Photon M3 Max (Fig. 2,20) is equipped with a 13.6-inch monochrome 7K LCD display and an advanced UV light matrix (Light Matrix 3.0), providing uniform illumination and high detail accuracy [71].

Fig.2.20 *Anycubic Photon M3 Max 3D printer*

2.5. Polymers and Composites for 3D Printing

3D printing using FFF allows the fabrication of polymer and composite materials with complex geometries and functional details unattainable with conventional methods. PLA, ABS, PA, PEEK and their composites with carbon fibers, graphite, graphene or natural fillers are commonly used, which increase the elastic modulus, compressive strength and stiffness, but at >15wt.% agglomeration and poor interlayer adhesion are observed. Mechanical properties depend strongly on the printing parameters (temperature, layer thickness, filament orientation, speed), as the materials are anisotropic and the strength along the Z axis is lower than that along the XY. Tribological characteristics include the coefficient of friction, wear (abrasive, adhesive, fretting, fatigue) and the influence of the structure from 3D printing [76–78].

2.5.1. Types of Plastics for 3D Printing

There are two main types of plastics used in 3D printing – thermoplastics and thermosets [50].

1. Thermosets are the most commonly used type of plastic [50]. The main characteristic that distinguishes them from thermosets is their ability to undergo multiple cycles of melting and solidification.

2. Thermosets (also called thermosets) remain in a permanent solid state after solidification.

Table 2.4 summarizes data from manufacturers [79] and calculated values used in this study.

a) PLA [(C3H4O2)n] easy to print, most widely used polymer; low printing temperature and low tendency to warp [50].
b) ABS - stronger than PLA, but more difficult to print; requires a heated bed due to tendency to warp [50].
c) PETG - modified PET; strong, durable, easy to print and often used instead of PLA/ABS.
d) TPE, TPU, TPC - Thermoplastic elastomers (TPE) are flexible, elastic materials. TPU is harder and easier to print than TPE; TPC offers better UV/chemical/heat resistance (up to ~150°C).
e) Nylon - (polyamide) very strong, flexible and impact resistant; hygroscopic, can be painted; used for functional parts.
f) PC (polycarbonate) is very strong, transparent and heat resistant (up to ~110°C); suitable for technical and automotive parts.
g) Exotic 3D printing filaments (Hybrid materials) - mixtures of a base polymer (usually PLA) and additives such as metal, wood, ceramic, carbon/glass fibers; give specific properties and surfaces.
h) Composites - they increase strength at low weight. Reinforcement is achieved through short or continuous fibers, most often carbon, as well as glass or Kevlar.

Table 2.4 *Characteristics of the filaments used*

Материал	Температура на топене	T° на печат на глава – nozzle	T° на работна зона /легло/ - bed	Speed	cooling	Якост на опън	Якост на огъване	Flexural modulus	Hardness	Плътност на материала	Плътност на материала на проба - експериментално			
											Цилиндър - 100% запълване	Плоча 120/60/10 - 20% запълване	Плоча 60/60/10 - 20% запълване	Сфера 9mm - 20% запълване
	°C	°C	°C	mm/s	°C	[MPa]	[MPa]	MPa		[g/cm³]	[kg/m³]	[kg/m³]	[kg/m³]	[kg/m³]
PLA (silver)	-	210- 230°C	45-60°	40- 100	-	63	74	1973	-	1.24	1145.91559	-	-	-
3DJAKE PETG	-	230-250	60-90	20-200	15-25'	61	68	2050	-	1.29	1145.91559	-	-	857.89
ColorFabb SteelFill	-	190-210	50-60	40-80	On	23	30	3000	-	3,13	2801.127	-	-	2786.84
Carbon Fil	-	± 230 - 265°				52.5	-	± 4600	109	1.19	1082.25361	-	-	1134.21
3DJAKE TPU A95	190 ± 10	200 – 230	60-90		15-25'	55	-	2303	95A	1.20	-	-	352.77	686.84
EasyFil™ HIPS (blue)	± 180 - 260° C	± 220 - 260	0-60	-	-	22	± 51.2		-	1.04	-	-	-	565.26
EasyFil™ HIPS (black)	± 180 - 260	220 - 260°	0-60	-	-	22	± 51.2	± 2126	-	1.04	-	-	416.666	703.15
ABS	235 ± 10	235 – 255	± 80	-	15-25	43,6	-	-	-	1,1	-	-	-	-

In Table 2.5, the most commonly used filaments and their characteristics are presented.

Table 2.5 *Types of filaments for 3D printing*

Вид	Сила	Гъвкавост	Издръжливост	Трудност при използване	Температура на печат	Температура на леглото за печат	Изкривяване	Разтворимост	Безопасност за храните
PLA	Висока	Ниска	Средна	Ниска	180°-230°	20°-60°	Минимално	Не	Указания на потребителя
ABS	Висока	Средна	Висока	Средна	210°-250°	80°-110°	Значително	В естери, кетони и ацетон	Не
PETG	Висока	Средна	Висока	Ниска	220°-250°	50°-75°	Минимално	Не	Указания на потребителя
TPE, TPU, TPC	Средно	Много висока	Много високо	Среден (TPE, TPC); Ниско (TPU)	210°-230°	30° – 60°	Минимално	Не	Не
НАЙЛОН	Висока	Висока	Висока	Средна	240°-260°	70°-100°	Значително	Не	Указания на потребителя
PC	Много висока	средна	Много висока	Средна	270 °–310°	90°-110°	Значително	Не	Не

2.5.2. Types of Resins for 3D Printing

Resin is a UV-curable photopolymer liquid used primarily in SLA, DLP, and PolyJet 3D printing. Under exposure to light, it solidifies layer by layer, producing models with high detail and smooth surface finish. A wide variety of resins is available, offering different properties: standard, rigid, water-washable, dental, flexible, castable, heat-resistant, as well as dyes and auxiliary additives for tuning material behavior.

2.6. EDEM Software

EDEM is a simulation software package specifically designed for modeling discrete elements and is widely used in engineering and scientific applications. It is particularly effective for analyzing mechanical systems involving particle dynamics. The software is suitable for simulating 3D-printed samples and calculating sliding friction, rolling friction, and restitution coefficients [80-85].

For the simulation modeling in this dissertation, the EDEM Software package (Discrete Element Method) was used. The suite includes several modules:

- **EDEM Creator** – for building object models,
- **EDEM Simulator** – for simulating interactions between multiple bodies,
- **EDEM Analyst** – for analyzing results, generating graphs, evaluating angles, number of grinding media, wear, and additional performance indicators [80-85].

2.7. Conclusion

Tribological testing provides essential data for the design, optimization of materials, surface treatments, and extending the lifetime of components. Rockwell hardness testing is especially important for assessing mechanical properties of soft materials while complying with international standards. Modern tribology is increasingly linked to 3D printing of polymers and composites, enabling rapid prototyping and more accurate prediction of material behavior under real operating conditions.

Different 3D printing technologies offer specific advantages:

- **FDM (Fused Deposition Modeling)** – the most accessible and widely used technology, suitable for prototypes and functional parts made of thermoplastic polymers. It enables fast production but has limitations in accuracy and surface finish.
- **PolyJet** – a high-resolution technology allowing the combination of multiple materials and hardness levels in a single printed part. Ideal for detailed models, medical applications, and components requiring elastic properties.
- **SLA (Stereolithography) and DLP (Digital Light Processing)** – provide exceptional accuracy and smooth surfaces through curing of photopolymer resins. Widely applied in dental medicine, prosthetics, and visually demanding parts.
- **SLS (Selective Laser Sintering)** – uses polymer powders to create strong and functional components suitable for industrial applications. Does not require support structures.
- **SLM (Selective Laser Melting) and DMLS (Direct Metal Laser Sintering)** – metal 3D printing technologies enabling the fabrication of complex and highly durable components for aerospace, automotive, and medical implants.
- **MJF (Multi Jet Fusion)** – offers high printing speed, good detail resolution, and excellent mechanical properties, making it suitable for series production of plastic parts.
- **Binder Jetting** – applies a liquid binder onto powder materials, allowing cost-efficient production of complex shapes and detailed geometries.

Combining tribological research with these advanced manufacturing technologies is crucial for proper evaluation of new materials—particularly polymers and composites, which are gaining

increasing importance in industry. This integration enables not only process optimization but also prediction of durability and material performance under real operating conditions.

Chapter 3.

Development of Methodologies for Conducting the Research

This chapter presents the development and justification of the methodologies used in the experimental studies of 3D-printed polymer and composite materials. The aim is to ensure precise, reproducible, and scientifically grounded results. Each methodology is tailored to the characteristics of the materials, the objectives of the study, and the technical capabilities of the equipment described in Chapter 2.

3.1. Methodologies for 3D Printing

The methodologies for 3D printing are adapted according to the type of printer, the printing technology, the geometry and features of the specimen, as well as the purpose of fabrication [198].

I. FDM Printing Technology

The methodology for FDM 3D printing begins with creating a CAD model, exported in STL format, which is then sliced in software that generates G-code. Depending on the series, the G-code is transferred to the printer via SD card (Tevo Tornado) or via network connection (Ultimaker S5). Before printing, the build plates are leveled and the nozzles are cleaned. The printing process proceeds layer by layer through material extrusion. Upon completion, the model is removed, post-processed, and inspected for defects and conformity to the specifications.

II. Stratasys Objet260 Connex3 – PolyJet Technology

Fabrication of the specimens using PolyJet technology (Stratasys) involved the following steps: The 3D models were created in CAD and exported in STL format, checked for correctness, and oriented for optimal accuracy. The files were prepared in GrabCAD Print/Objet Studio by selecting the photopolymer (Vero/Tango/Digital ABS), the High Quality mode, and automatic generation of support material. The printer was configured, the material cartridges and print heads were inspected, and printing was performed layer by layer (16–30 μm) with UV curing. The support material was removed mechanically or using an alkaline solution with ultrasound, followed by rinsing and drying.

III. Anycubic Photon M3 Max – LCD/SLA Technology

Specimens fabricated with the Anycubic Photon M3 Max (LCD/SLA) were prepared as follows: The 3D models were created in CAD and exported in STL. In the Anycubic Photon Workshop software, the orientation, layer quality, and supporting structures were defined. Printing was carried out layer by layer through UV curing of the photopolymer. After printing, the models were cleaned with isopropyl alcohol and post-cured with UV light using the Anycubic Wash and Cure 3 Plus.

3.1.1. Development of a Methodology for 3D Printing of Plates

The geometric plates were created in 3D Builder (Microsoft) as rectangular parallelepipeds with dimensions 120 × 60 × 10 mm and 60 × 60 × 10 mm (Fig. 3.1 and Fig. 3.2), after which they were processed for printing and manufactured using the selected 3D printing technology.

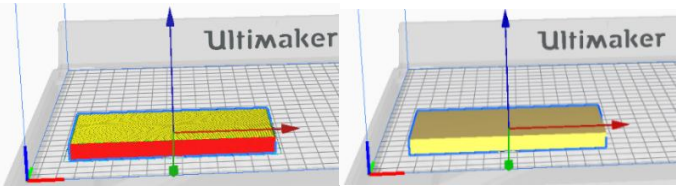

Fig. 3.1. *Modeling of a plate with dimensions 120/60/10 mm.*

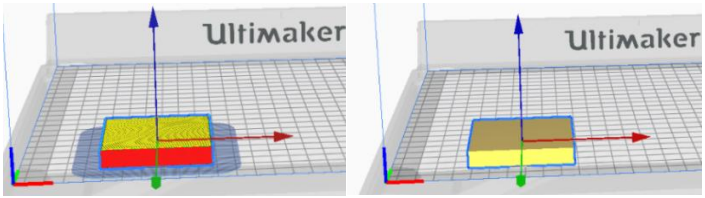

Fig. 3.2. *Modeling of a plate with dimensions 60/60/10 mm.*

The geometric plates (120×60×10 mm and 60×60×10 mm) were created in 3D Builder and exported as STL files. In Ultimaker Cura, the models were positioned horizontally with a layer height of 0.2 mm, 20% infill, a "Zig-Zag" or "Triangles" pattern, appropriate nozzle and bed temperature, a printing speed of ~50 mm/s, and Brim/Skirt enabled. After the settings were finalized, G-code was generated for the printer.

3.1.2. Development of a methodology for 3D printing cylinders

For the study of the tribological properties of the used filaments, cylindrical samples with dimensions h = 20 mm and r = 5 mm were prepared (Fig. 3.3).

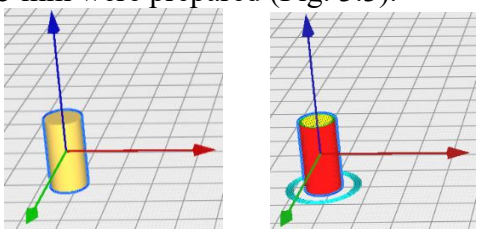

Fig. 3.3 *Modeling of cylinders in a software environment*

The methodology for 3D printing cylindrical specimens includes creating a CAD model, converting it into STL format for slicing. The materials used are PLA, SteelFeel, or CarbonFill with optimized parameters—layer thickness of 0.1–0.2 mm, appropriate nozzle and bed temperature, 100% infill, and a base (brim or raft). Due to the simple geometry of the cylinder, no supports are required. The experimental specimen has a height of 20 mm and a radius of 5 mm.

3.1.3. Development of a methodology for 3D printing spherical bodies

The methodology for 3D printing spherical specimens includes creating a CAD model, converting it into STL format, and printing via FDM using optimized parameters—layer thickness, temperature, and object orientation. Due to the stepping effect and the limited support area, support structures are used, and in some cases SLA technology is applied. The materials used are PLA, SteelFeel, and CarbonFill with 100% infill. The spheres, with a diameter of 9 mm, are printed three at a time. After printing, the supports are removed and the objects may undergo additional post-processing. Figures 3.4 and 3.5 show the spheres with five types of bases—none, Brim, Raft, Skirt + Support, and Raft + Support, while the data for material consumption and printing time are summarized in Table 3.1.

Table 3.1. *Amount of material used and printing time*

	Tevo Tornado		Ultimaker S5	
Тип „подложка“	Време, min	К-во суровина,g	Време, min	К-во суровина,g
None	19	1	10	1
Brim	20	2	13	1
Raft	27	3	18	2
Raft support	30	3	20	2
Skirt support	20	2	12	1

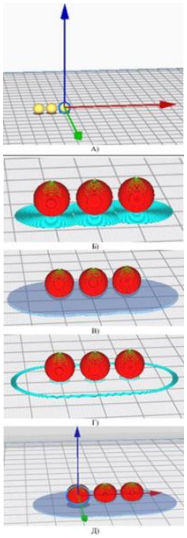

***Figure 3.4**. Modeling of spheres with different build plates: A) without a build plate; B) with a Brim; C) with a Raft; D) with Skirt + Support; E) with Raft + Support used for printing.*

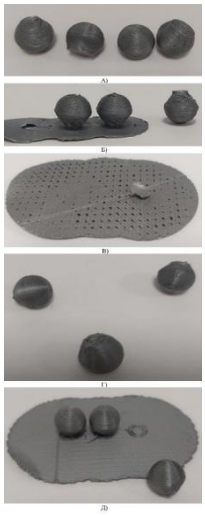

***Figure 3.5.** Printed spheres with different build plates: A) without a build plate; B) with a Brim; C) with a Raft; D) with Skirt + Support; E) with Raft + Support.*

3.2. Methodology for Microhardness Analysis of Polymers and Composites

Three methodologies were developed for the investigations, using the equipment described in Chapter 2, Section 2.2. The testing was conducted with the EBP BRV-187.5T hardness tester, followed by measurement of the indentations using the Olympus BX53M + DP23 system.

- **Instruction Manual Digital Shore Hardness Tester SAUTER HD**
  Shore microhardness measures the hardness of polymers and elastomers by evaluating the material's resistance to penetration by a rigid indenter. The measurement is performed using a digital durometer Sauter HD on 3D-printed specimens and is reported in Shore units (Shore A, D, etc.). The method is suitable for thin and highly elastic materials.

Figure 3.6. *Shore microhardness measurement device (described in Chapter 2).*

- **Hardness Tester EBP BRV-187.5T (described in Chapter 2)**
  Prior to testing, calibration and verification of the device are performed. The load and the indenter of the hardness tester are checked using certified reference blocks (steel, nickel, or polymer) to confirm proper load-cell functioning and closed-loop operation. The optical system is calibrated using a stage micrometer, and for each objective (10×, 20×, 50×, etc.), a corresponding conversion factor (μm/px) is determined and recorded.

  For the test, the Rockwell method is selected, using an HRR/60/12.7 indenter, a test force of **F = 60 kgf**, and a loading time of **1 s**. The EBP BRV-187.5T is set to the appropriate mode, the workspace is isolated from vibrations, and the specimen is leveled horizontally to ensure uniform loading during indentation.

3.3. Methodology for Investigating Tribological Properties of Polymers and Composites Produced by 3D Printing

For the purposes of this dissertation, polymer and composite specimens produced by 3D printing were examined using newly developed methodologies for studying the following tribological properties:

- sliding friction coefficient,
- rolling friction coefficient,
- coefficient of restitution.

The investigation includes:

1) Sliding friction:
Kinetic friction is the contact force resisting the sliding motion between an object and a surface. It is typically lower than static friction, which facilitates movement once motion has already begun [86]. The kinetic friction force is determined by:

$$Fk = \mu k.N \tag{3.1}$$

Where:

Fk is the kinetic friction force;
μk is the coefficient of kinetic friction;
N is the normal force.

When a force is applied to a block on an inclined plane, its acceleration depends on the relationship between the external force and the kinetic friction force. The block accelerates if the external force exceeds the friction force, stops or decelerates if friction is greater, and moves at constant velocity when the two forces are equal, according to Newton's first law. The principle is illustrated in Fig. 3.7 by a free-body diagram.

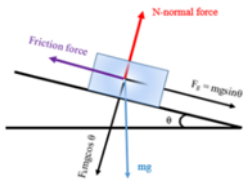

Figure 3.7 *Free-body diagram of a block subjected to friction while sliding on an inclined surface*

[87]

The component of gravity along the incline is given by:

$$Fg = mgsin\theta \tag{3.2}$$

Where:

m is the mass of the block,
g is the gravitational acceleration,
θ is the angle of inclination.

The normal force (perpendicular to the surface) is given by:

$$N = mgcos\theta \tag{3.3}$$

Therefore, since the friction force opposes the motion of the block:

$$Fk = \mu k \, . \, mgcos\theta \tag{3.4}$$

The coefficient of kinetic friction on an inclined plane is determined when the component of the force parallel to the surface acting on the block is equal to the perpendicular force. This occurs at a specific angle θ at which the block moves at constant velocity:

$$\Sigma F = ma = 0 \tag{3.5}$$

$$Fk = Fg \; or \; \mu kmgcos\theta = mgsin\theta \tag{3.6}$$

From the above equations it follows that:

$$\Sigma\mu k = mgsin\theta/mgcos\theta = tan\theta \tag{3.7}$$

Where θ is the angle at which the block begins to move with constant velocity [88].

2) Rolling friction

Rolling friction occurs when an object moves over a surface and encounters resistance due to kinetic friction at the contact point. The weight, roughness, and elasticity of both the object and the surface can cause deformations that generate the friction force [89].

Figure 3.8 illustrates rolling friction on an inclined plane, where the normal force depends on the cosine of the angle between the weight and the direction perpendicular to the surface (equation 3.8):

$$Fr\theta = fWcos\theta \tag{3.8}$$

Where:

Fr is the rolling friction force at angle θ;
θ is the angle of inclination.

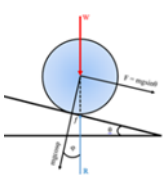

Figure 3.8 *Rolling friction [90]*

3) Coefficient of restitution

To investigate the influence of friction and the coefficient of restitution, a methodology was developed in which 3D-printed spheres are dropped freely onto flat specimens. The goal is to determine the restitution coefficient, calculated as the ratio between the rebound height and the drop height. The spheres (Ø 9 mm) were manufactured from HIPS, TPU, PLA, PETG, Carbon, Vero White, and others, with a steel sphere used for comparison. Corresponding plates with dimensions 60 × 60 × 10 mm were printed for each material.

The samples are released from a height of 650 mm using a guiding tube, and the impact is recorded with a high-speed camera NAC MEMRECAM HX-6 at 500 fps. Using Vicasso 2009 software, the height of the first rebound is determined, with three repetitions performed for each combination and the results averaged.

The obtained values of the restitution coefficient are presented in tabular form (Chapter 4, Section 4.1.3) and are used as input data for simulations of the motion of grinding bodies in mills. This enables more accurate modelling of key parameters and optimization of the energy efficiency of the process.

3.4. Methodology for creating a simulation in EDEM Software

In the Creator module of EDEM Software, the input parameters for simulation modelling are defined, as shown in Figure 3.9. The process begins with specifying the particle material (Bulk material), including friction and rolling friction coefficients, restitution, density, and size. Next, a material is created for the equipment (Equipment material). In the *Geometries* section, geometries can be generated directly in the software or imported as existing CAD models [80–85], with assigned actions such as translation, rotation, velocity, acceleration, and action time.

This is followed by creating a *Factory* for generating the particles with predefined properties and quantity (number, mass, or unlimited), as well as parameters such as production time, start time, contact limits, and more. For the simulations, the standard Hertz–Mindlin contact model was selected.

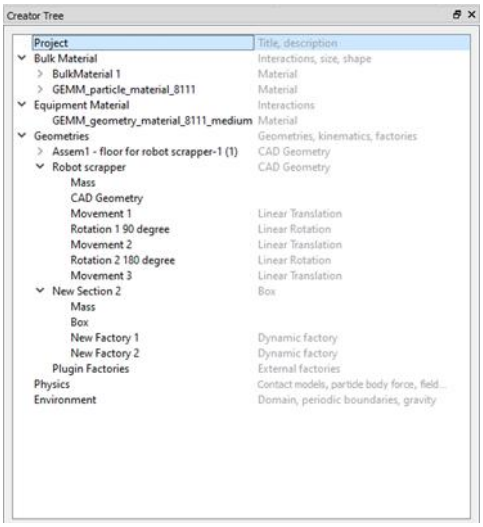

Figure 3.9 *Input parameters for simulation modeling*

For the purposes of simulation modeling with EDEM Software, the following methodology was established: defining the goal and task; defining particles – type, size, physical properties; defining and positioning geometry – type, size, physical properties, file format selection; defining and positioning a Factory for particle generation; creating a trajectory; and creating models for analyzing the simulation output data.

The goal of the simulation modeling is to create a unified model to study various types of polymers and composites obtained via 3D printing, focusing on the restitution coefficient. The tasks to be completed include: particle creation, geometry positioning, trajectory creation, and analysis of data obtained from the simulation modeling.

3.5 Conclusion

The tribological properties of 3D-printed polymers require further investigation and optimization of manufacturing parameters for applications in industries such as automotive, aerospace, medical, and construction. The conducted studies demonstrate the potential of 3D-printed polymers, and further technological development will improve their tribological performance.

This chapter systematizes methodologies for experimental studies of 3D-printed polymeric and composite materials. The developed approaches ensure reproducibility, consistency, and high reliability of data, allowing a comprehensive assessment of the tribological and mechanical properties of the specimens.

The 3D printing methodology guarantees high geometric accuracy and structural uniformity of the samples, while microhardness analysis via Brinell and Shore provides precise evaluation of local mechanical properties. The methodology for tribological studies allows determination of friction coefficients under sliding, rolling, and restitution, providing a reliable basis for validating simulation models.

Simulation modeling in EDEM Software complements the experimental studies, enabling virtual experiments, prediction, and optimization of technological parameters.

In summary, the developed methodologies form an integrated experimental-analytical system that ensures comparability between experimental and simulation results and provides a methodological foundation for data analysis and interpretation, as well as for optimization of technological processes in 3D printing of polymers and composites.

Chapter 4

Experimental Results and Investigations of 3D-Printed Polymer Materials, Including Composites

This chapter summarizes the results of experimental studies on 3D-printed polymer and composite materials with different geometries – flat tiles, cylinders, and spheres. The aim is to evaluate the influence of shape, technological parameters, and composition on the tribological and mechanical properties of the materials.

4.1 Results of Friction Coefficient Studies of 3D-Printed Samples

Within the experimental studies, the mechanical and tribological properties of 3D-printed polymer and composite materials were analyzed. Samples from different materials were compared, prepared with parameters ensuring high geometric reproducibility and structural homogeneity. Figures 4.1 and 4.2 show samples of HIPS (High Impact Polystyrene) and TPU (Thermoplastic Polyurethane).

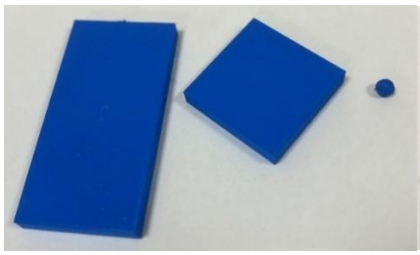

Figure 4.1 *Samples for HIPS testing*

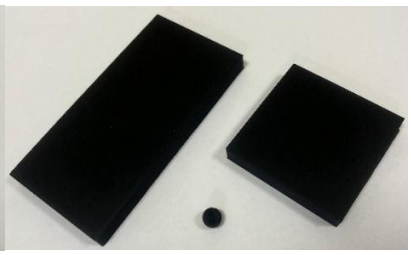

Figure 4.2 *Samples for TPU testing*

The results of tribological studies on EasyFil HIPS (Dark Blue) during 3D printing are presented, including comparative analysis with other filaments [91]. The interaction of HIPS with PLA, PETG, CARBON, Steel Fil, TPU, Flex, and Vero White was investigated by measuring sliding friction, rolling friction, and the restitution coefficient. Based on the experimental data for TPU and HIPS, simulation models were created for verification and the development of more accurate models of interactions between milling media and the grinding environment.

4.1.1 Coefficient of Sliding Friction

This section presents the results of experimental studies according to the methodology described in Chapter 3, aimed at analyzing the influence of various parameters on the measured values for polymers and composites produced via 3D printing.

First, the kinetic friction data were processed using equations (3.1)–(3.7). The obtained coefficients of kinetic friction for different inclinations and surfaces are summarized in a table showing the dependence between the slope angle and block movement. Figure 4.3 illustrates the six measurements used to determine the sliding angle.

Figure 4.3. *Images from the experiment to determine the coefficient of sliding friction*

Table 4.1 contains the measured angles in degrees and radians, as well as the calculated coefficient of sliding friction for the material EasyFil HIPS (Dark Blue) in contact with itself (HIPS+HIPS). In addition, a comparative analysis was performed with two other widely used 3D-printed materials – PLA+PLA and PETG+PETG – to evaluate differences in tribological behavior during sliding.

Table 4.1. *Coefficient of sliding friction for HIPS+HIPS and comparative analysis with PLA+PLA and PETG+PETG*

Material (plate 120×60×10 mm + plate 60×60×10 mm)	**Friction angle, θ⁰**	**Friction angle, θ rad**	**Coefficient of sliding friction, tg θ⁰**
Hips+Hips (1)	25,01	0,436507	0,46652
Hips+Hips (2)	22,06	0,38502	0,405245
Hips+Hips (3)	23,68	0,413294	0,438553
Hips+Hips (4)	19,98	0,348717	0,363575
Hips+Hips (5)	23,64	0,412596	0,437721
Hips+Hips (6)	24,23	0,422893	0,450047
Hips+Hips avg	23,1	0,403171	0,426536
PLA+PLA (1)	15,850	0,277	0,284
PLA+PLA (2)	19,610	0,342	0,356
PLA+PLA (3)	22,590	0,394	0,416
PLA+PLA avg	19,350	0,338	0,351
PETG+PETG (1)	21,300	0,372	0,390
PETG+PETG (2)	20,810	0,363	0,380
PETG+PETG (3)	24,430	0,426	0,454

Within the study, the interaction of EasyFil HIPS with various commonly used 3D-printed materials—PLA, PETG, CARBON, Steel Fil, TPU, Flex, and Vero White—was evaluated. Figure 4.4 shows photos from the experiment to determine the coefficient of sliding friction. Eight samples (60×60×10 mm) of different materials (HIPS, PLA, PETG, Carbon, Steel Fill, Vero White, Flex, TPU) were slid over a 120×60×10 mm HIPS plate.

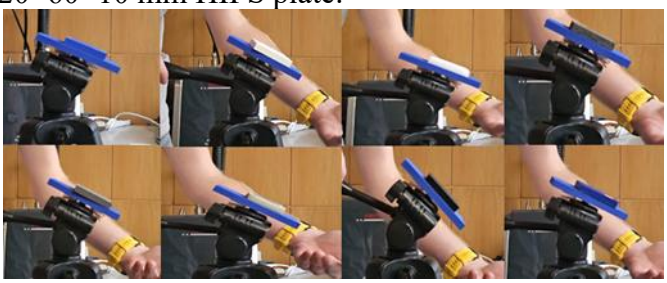

Figure 4.4. *Photos from the experiment to determine the coefficient of sliding friction.*

Table 4.2 presents the results of the study for determining the sliding friction coefficient of the materials HIPS, PLA, PETG, Carbon, Steel Fill, Vero White, Flex, and TPU.

Table 4.2*. Experimental results for the coefficient of sliding friction for HIPS (120×60×10 mm) + material (60×60×10 mm – HIPS, PLA, PETG, Carbon, Steel Fill, Vero White, Flex, TPU).*

Material (plate 120×60×10 mm + plate 60×60×10 mm)	**Friction angle, θ⁰**	**Friction angle, θ rad**	**Coefficient of sliding friction, tg θ⁰**
Hips 1	25,61	0,446979	0,479334
Hips 2	24,91	0,434762	0,464397
Hips 3	23,01	0,4016	0,424681
avg	24,51	0,42778	0,455937
PLA 1	26,04	0,454484	0,488597
PLA 2	28,2	0,492183	0,536195
PLA 3	31,41	0,548208	0,610642

Material (plate 120×60×10 mm + plate 60×60×10 mm)	Friction angle, θ⁰	Friction angle, θ rad	Coefficient of sliding friction, tg θ⁰
avg	28,55	0,498292	0,544086
PETG 1	24,07	0,420101	0,446693
PETG 2	21,78	0,380133	0,399567
PETG 3	20,92	0,365123	0,382263
avg	22,25667	0,388452	0,409247
Carbon 1	25,38	0,442965	0,474407
Carbon 2	28,41	0,495848	0,540924
Carbon 3	26,48	0,462163	0,498146
avg	26,75667	0,466992	0,504187
Steel fill 1	21,98	0,383623	0,40362
Steel fill 2	27,79	0,485027	0,527017
Steel fill 3	31,28	0,545939	0,607532
avg	27,01667	0,47153	0,509892
Vero white 1	30,35	0,529707	0,585524
Vero white 2	31,01	0,541227	0,601098
Vero white 3	29,03	0,506669	0,554994
avg	30,13	0,525868	0,580379
Flex 1	46,49	0,811404	1,053412
Flex 2	47,27	0,825017	1,082552
Flex 3	50,38	0,879297	1,207934
avg	48,04667	0,838573	1,112433
TPU 20% 1	24,43	0,426384	0,454252
TPU 20% 2	25,63	0,447328	0,479764
TPU 20% 3	25,57	0,446281	0,478476
avg	25,21	0,439998	0,470777

Figure 4.5 *Photo from the experiment for determining the coefficient of sliding friction TPU+HIPS.*

Table 4.3 *Coefficient of sliding friction for TPU + materials (60×60×10 mm – HIPS, PLA, PETG, Carbon, Steel Fill, Vero White, Flex, TPU).*

Material (plate 120×60×10 mm + plate 60×60×10 mm)	Friction angle, θ⁰	Friction angle, θ rad	Coefficient of sliding friction, tg θ⁰
Hips 1	25.61	0.446979	0.479334
Hips 2	24.91	0.434762	0.464397
Hips 3	23.01	0.4016	0.424681
avg	24.51	0.42778	0.455937
PLA 1	26.04	0.454484	0.488597
PLA 2	28.2	0.492183	0.536195
PLA 3	31.41	0.548208	0.610642
avg	28.55	0.498292	0.544086
PETG 1	24.07	0.420101	0.446693
PETG 2	21.78	0.380133	0.399567

Material (plate 120×60×10 mm + plate 60×60×10 mm)	Friction angle, θ⁰	Friction angle, θ rad	Coefficient of sliding friction, tg θ⁰
PETG 3	20.92	0.365123	0.382263
avg	22.25667	0.388452	0.409247
Carbon 1	25.38	0.442965	0.474407
Carbon 2	28.41	0.495848	0.540924
Carbon 3	26.48	0.462163	0.498146
avg	26.75667	0.466992	0.504187
Steel fill 1	21.98	0.383623	0.40362
Steel fill 2	27.79	0.485027	0.527017
Steel fill 3	31.28	0.545939	0.607532
avg	27.01667	0.47153	0.509892
Vero white 1	30.35	0.529707	0.585524
Vero white 2	31.01	0.541227	0.601098
Vero white 3	29.03	0.506669	0.554994
avg	30.13	0.525868	0.580379
Flex 1	46.49	0.811404	1.053412
Flex 2	47.27	0.825017	1.082552
Flex 3	50.38	0.879297	1.207934
avg	48.04667	0.838573	1.112433
TPU 20% 1	24.43	0.426384	0.454252
TPU 20% 2	25.63	0.447328	0.479764
TPU 20% 3	25.57	0.446281	0.478476
avg	25.21	0.439998	0.470777

4.1.2. Coefficient of Rolling Friction

The results of the experimental determination of the rolling friction coefficient on an inclined surface are presented. Measurements were carried out at different incline angles θ\thetaθ, and for each series of tests, the corresponding friction force was recorded and calculated using formula (3.8). Based on the obtained data, the rolling friction coefficient was determined, and the results are summarized in Table 4.4 and shown in Figure 4.6.

Figure 4.6: *Photos from the experiment for determining the rolling friction coefficient.*

Figure 4.6 shows images from the experiment for each material – PLA, PETG, Carbon, Steel Fill, Vero White, and Steel. Table 4.4 presents the results of the study, where three trials were conducted for each material, and the average rolling friction coefficient is reported. It was found that the interaction of HIPS with PETG produced the highest rolling friction coefficient (0.31344), while the lowest was observed with Steel (0.179604).

Table 4.4 *Results of rolling friction coefficient measurements for HIPS plate + sphere of the listed materials.*

Material (HIPS plate + sphere of materials)	Friction angle, θ⁰	Friction angle, θ rad	Rolling friction coefficient, sin θ⁰
Hips 1	6,33	0,110479	0,110255
Hips 2	7,94	0,138579	0,138136
Hips 3	17,21	0,300371	0,295875
avg	10,49333	0,183143	0,182121

PLA 1	11,95	0,208567	0,207058
PLA 2	15,51	0,270701	0,267407
PLA 3	18,04	0,314857	0,309681
avg	15,16667	0,264708	0,261628
PETG 1	16,53	0,288503	0,284517
PETG 2	18,29	0,319221	0,313827
PETG 3	19,98	0,348717	0,341692
avg	18,26667	0,318813	0,31344
Carbon 1	10,59	0,18483	0,18378
Carbon 2	15,19	0,265116	0,262021
Carbon 3	17,63	0,307702	0,302869
avg	14,47	0,252549	0,249873
Steel fill 1	13,74	0,239808	0,237516
Steel fill 2	21,64	0,377689	0,368774
Steel fill 3	10,45	0,182387	0,181377
avg	15,27667	0,266628	0,26348
Vero white 1	14,06	0,245393	0,242938
Vero white 2	6,99	0,121999	0,121696
Vero white 3	12,15	0,212058	0,210472
avg	11,06667	0,19315	0,191951
Steel 1	8,16	0,142419	0,141938
Steel 2	9,21	0,160745	0,160053
Steel 3	13,67	0,238587	0,236329
avg	10,34667	0,180583	0,179604

4.1.3. Coefficient of Restitution

To determine the coefficient of restitution, three experiments are conducted for each material, and the average value is taken. The experimental results are presented in Table 4.5. The coefficient of restitution is calculated using the formula [91]:

$$e = \frac{v_2}{v_1} = \left(\frac{h_2}{h_1}\right)^{\frac{1}{2}} \quad (9)$$

Where:

e - coefficient of restitution;
v_2 - velocity after rebound;
v_1- velocity before rebound;
h_1- height before rebound;
h_2- height after rebound.

Figure 4.7 *Photos from the experiment to determine the coefficient of restitution*

Table 4.5 *Coefficient of restitution for HIPS plate + spheres made of the specified materials*

Material (Base/Sphere)	№	Initial height [mm]	Rebound height [mm]	D/C	e – Coefficient of restitution SQRT D/C
Hips/Hips	1	650	320,41	0,492938	0,702096
	2	650	94,47	0,145338	0,381233
	3	650	67,65	0,104077	0,32261
	avg	650	160,8433	0,247451	0,497445
Hips/Carbon	1	650	281,9	0,433692	0,658553
	2	650	250,34	0,385138	0,620595
	3	650	238,13	0,366354	0,605272
	avg	650	256,79	0,395062	0,628539
Hips/PETG	1	650	180,97	0,278415	0,527651
	2	650	234,41	0,360631	0,600525
	3	650	369,51	0,568477	0,753974
	avg	650	261,63	0,402508	0,634435
Hips/PLA	1	650	255,67	0,393338	0,627167
	2	650	293,08	0,450892	0,671485
	3	650	315,73	0,485738	0,696949
	avg	650	288,16	0,443323	0,665825
Hips/Steel	1	650	354,57	0,545492	0,738575
	2	650	313,39	0,482138	0,694362
	3	650	339,75	0,522692	0,722975
	avg	650	335,9033	0,516774	0,71887
Hips/Steel fill	1	650	277,17	0,426415	0,653005
	2	650	313,43	0,4822	0,694406
	3	650	248,4	0,382154	0,618186
	avg	650	279,6667	0,430256	0,655939
Hips/Vero White	1	650	208,98	0,321508	0,567016
	2	650	268,56	0,413169	0,642782
	3	650	171,42	0,263723	0,51354
	avg	650	216,32	0,3328	0,576888

4.1.4. Investigation and Application of Tribological Characteristics of 3D Printed Materials for Tactile Perception of Visually Impaired People

3D technologies create new opportunities to improve access for visually impaired individuals to information and cultural heritage through the production of tactile objects, Braille inscriptions, and educational models [92].

Tribological factors such as surface roughness, durability, and layer height were studied on 3D printed PLA and Visijet PXL Core materials. The results indicate that high resolution (0.06 mm) and contour widths around 1 mm provide the best tactile perception.

The developed models have been implemented at Sofia University “St. Kliment Ohridski” [93].

Results:

- Surface smoothness and low roughness are critical for positive tactile perception. Objects printed with PLA at high resolution (0.06 mm) are evaluated as the smoothest and easiest to recognize.
- Contour reliefs with a width of about 1 mm provide the best tactile durability and shape recognition. Thinner contours (0.5 mm) are too fine, while thicker ones (1.2 mm) are perceived as coarse and hinder detail recognition.
- For Braille inscriptions, optimal perception corresponds to standard font sizes. Larger sizes are suitable for people who rarely read Braille.
- Some objects of cultural and historical heritage (Sphinx, Isis) are difficult to recognize for blind participants, whereas simpler shapes (animals, house, car) are more easily identified.
- Tribological surface properties (touch friction force, uniformity, roughness) directly affect the ease and speed of recognition.

The tactile suitability of 3D printed materials for visually impaired individuals was examined. Materials were produced using FDM (PLA) and ColorJet (gypsum material with various coatings) technologies.

Various 3D models were created, including Egyptian symbols, animals, cars, Braille alphabet, and educational and game objects (Fig. 4.8). Five blind participants and four visually impaired individuals evaluated the models by touch. The results helped determine suitable materials and technologies for creating tactile educational and cultural models.

Details from Fig. 4.8 a) to f) were printed using FDM technology, while Fig. 4.8 g) was printed using CJP technology.

PLA material was 3D printed via FDM under the following parameters: 20% infill, 3 external walls, bed temperature 60 °C, nozzle temperature 215 °C, speed 60 mm/s, and layer height 0.06 mm or 0.2 mm.

Details such as the goddess Isis, the Braille alphabet, and the globe were printed at high resolution (0.06 mm), while the Sphinx, owl, and animal models were printed at 0.2 mm.

The object in Fig. 4.8 g was produced in 6 variants, treated with a different number of Color Bond™ 30 coatings (from 2 to 6 layers), with one left untreated.

Two groups of young visually impaired participants took part in the experiment – one with progressive vision loss, and the other congenitally blind. During the tests, some models were described, some were not, and others were given incorrect instructions to assess recognition ability.


a) b)

c)


d) e)

f) g)

Figure 4.8. *3D Printed Samples*

Studies aimed at understanding how to "read" a picture were conducted by exploring a real 3D model by touch (Fig. 4.9 a), after which the model was converted into a tactile image (Fig. 4.9 b).

Tribological factors such as material roughness and layer height of 3D printed objects were investigated, as the specialized literature contains extensive research on the influence of these factors, particularly in relation to works of art.

For the tactile plate, the following object factors were observed: contour height, contour width, and perception.

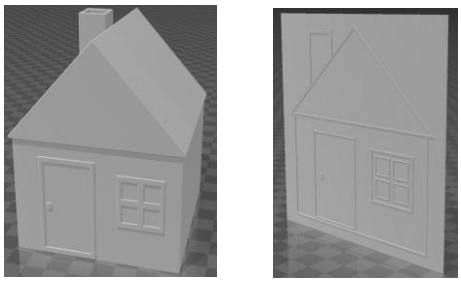

a) 3D model of a house b) 2D tactile version

Figure 4.9. *3D model of a house*

The aim of the study is to determine which details, fonts, and line thicknesses are most suitable for tactile perception. The figures of the goddess Isis (Fig. 4.8 a) and the Sphinx (Fig. 4.8 b) were recognized by visually impaired individuals but not by those who are completely blind. The owl figure (Fig. 4.8 g) was successfully identified by both partially sighted and blind participants with the aid of a verbal cue; the larger model was found to be more convenient for tactile orientation.

Minimal differences in surface texture were observed between details printed at different resolutions (0.06–0.2 mm), with all models being recognizable, and the finest figure being the smoothest. Defects at the bottom were associated with the support material used during printing. Egyptian figures were not recognized by blind participants, whereas Braille letters (Fig. 4.8 c) were clear and easy to read. The most suitable size for experienced readers is 18 pt, while beginners benefit from 20–22 pt.

Figure 4.10. *3D printed Braille text*

4.2. Results from the Study of Material Microhardness

For measuring microhardness using the Shore method, flat samples were 3D printed and then pressed with a hardness tester (Instruction Manual Digital Shore Hardness Tester SAUTER HD) on the test stand. Table 4.6 presents the results for density and Shore A hardness of the tested materials as the arithmetic mean of three measurements.

Table 4.6. *Results of density and Shore A hardness for the tested 3D materials*

Material	Density, g/cm^3	Shore A Hardness
PLA	1.1459	94.4
PETG	1.1459	79.3
HIPS	0.9563	71.7

Figure 4.11 presents a diagram of Shore hardness based on the data from Table 4.6. The highest hardness is observed for the PLA material, while the lowest is for HIPS, which also has the lowest density.

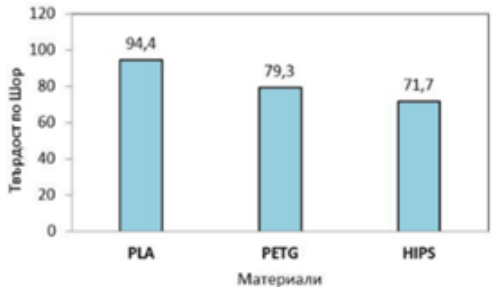

Figure 4.11 *Diagram of hardness of the tested materials*

For the microhardness study using the EBP BRV-187.5T durometer, two types of test specimens were modeled – plates (Figure 4.12) and cylinders (Figure 4.13), designed in Anycubic Photon Workshop. The software allows optimization of 3D models for photopolymer printing and control over geometry and orientation during printing.

The plates, with small thickness and a uniform surface, are used to evaluate surface hardening, while the cylinders, with a larger volume, allow analysis of the effect of UV treatment on bulk structures. All specimens were printed and processed under identical parameters, ensuring comparability and reliability of the results.

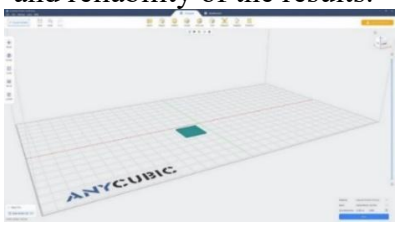

Figure 4.12 *Modeled plate with dimensions 20×20 mm and thickness 1 mm*

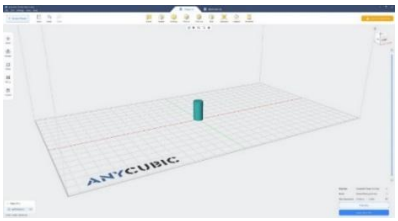

Figure 4.13 *Modeled cylinder with height 20 mm and diameter 10 mm*

The choice of these two geometries was made for two main reasons:

1) The different shapes and sizes allow investigation of the influence of UV treatment on surface hardness for objects with varying thickness and volume, thus assessing the effect of geometry on the degree of hardening.
2) The shapes were selected with practical applications in mind – the plates (Figure 4.14 a) resemble tactile navigation tiles, while the cylinders (Figure 4.14 b) can be used to create tactile elements for visually impaired people [94].

The aim of the experiments is to achieve higher surface hardness to increase the wear resistance and durability of these elements in real use.

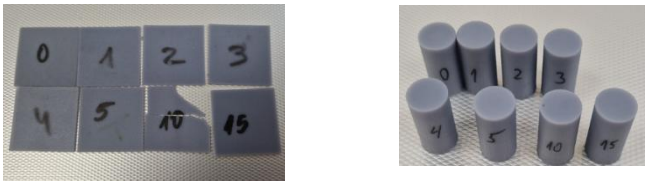

A) **B)**

Figure 4.14 *Tested samples of Resin 3D material, A) plates, B) cylinders.*

The hardness tester described in Chapter 2, EBP BRV-187.5T, was used to obtain the results. For the purposes of the study and the conducted experiments, the Rockwell scale HRR 60 with a 12.7 mm diameter indenter (Figure 4.15) was selected.

Figure 4.15 *Indenter with a diameter of 12.7 mm*

Figure 4.16 shows the screen of the control panel of the EBP BRV-187.5T hardness tester during the setup of testing parameters. The display allows input of key data – sample number, radius of curvature, measurement range, selected hardness scale, conversion type, and dwell time. After configuring the parameters, the test is started with the Start button. The intuitive interface provides precise control over measurement conditions and ensures high accuracy and repeatability of the results.

Figure 4.16 *Control panel of the EBP BRV-187.5T hardness tester*

Figure 4.17 shows the EBP BRV-187.5T hardness tester used to determine the surface hardness of the samples. The device is equipped with an indenter and a digital display with an intuitive interface, allowing the selection of the appropriate Rockwell scale (HRA, HRB, HRC, etc.) depending on the material and geometry of the samples.

Figure 4.17 *EBP BRV-187.5T hardness tester with mounted indenter used in the study.*

Table 4.7 and Figure 4.18 present the results of surface hardness testing of photopolymer tiles measuring 20 × 20 × 1 mm (Figure 4.14 a), printed with an Anycubic printer and exposed to UV light. It was found that hardness increases with UV curing time, with the optimal result achieved after 15 minutes. Longer exposure does not lead to significant changes, making the 15-minute treatment the most effective in terms of time, energy, and surface quality.

Table 4.7 *Hardness testing of a resin tile with dimensions 30 × 30 mm and thickness 1 mm.*

Resin UV Time [min]	***Rockwell HRR 60 (12.7 mm) ball***
0	30.2
1	53.1
2	62.3
3	69.6
4	73.4
5	81.3
10	87.6

15	90.5
20	92.6
25	92.7
30	93.8
35	93.3
40	92.1
45	93.5
50	93.4
55	94.3
60	94.4

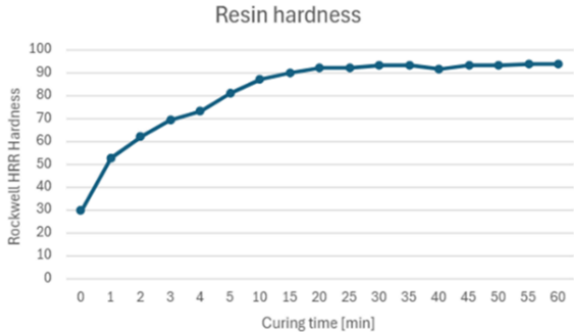

Figure 4.18 *Hardness testing of a resin tile with dimensions 20 × 20 mm and thickness 1 mm from Table 1, presented graphically.*

For cylindrical samples with a height of 20 mm and diameter of 10 mm (Figure 4.14 b), significant differences compared to flat samples are observed. The data (Table 4.8, Figure 4.19) show that prolonging UV exposure does not significantly increase surface hardness, which remains stable.

The reason is the limited penetration of UV light into massive structures – the inner layers remain partially polymerized, and the overall hardness does not increase substantially. These results emphasize the need to adjust UV curing parameters according to the geometry and thickness of the parts, as the effect is strong for thin objects but limited for bulkier ones, potentially leading to uneven mechanical properties.

Table 4.8 *Hardness testing of a cylinder with height 20 mm and diameter 10 mm, made of resin.*

Resin UV Time [min]	***Rockwell HRR 60 (12.7 mm) ball***
0	87.7
1	93.3
2	92.4
3	84.3
4	99.4
5	90.2
10	99.7
15	99.3
20	100.8
25	101.8
30	95.1
35	99.7
40	98.9
45	103.6

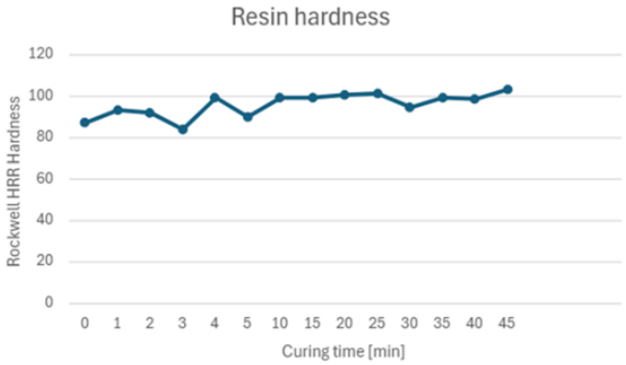

Figure 4.19 *Hardness testing of a cylinder with a height of 20 mm and a diameter of 10 mm, made of resin, presented in graphical form.*

UV treatment increases only the surface hardness of the resin samples, without affecting their internal structure. Analysis with a 3D computer tomograph Nikon XT-H 225 shows uniformity and consistent layer thickness (Figure 4.20).

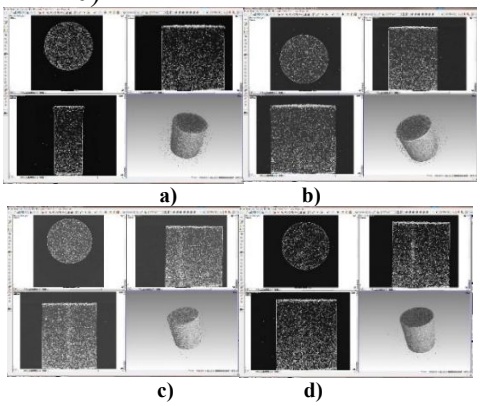

Figure 4.20 *Cross-sections of four cylinders with 3D reconstruction via computer tomography: a) No. 0, b) No. 5, c) No. 10, d) No. 15 (all from Figure 4.19 b).*

4.3. Simulation studies of 3D-printed samples using EDEM software

The experimental setup used for the tests is shown in Figure 4.21. The 3D-printed sphere (1) is placed in a chute (2) and then positioned on a plate (3). When the plate (3) is removed, the sphere (1) falls freely from a height of h1 = 540 mm onto the 3D-printed plate (4).

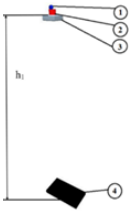

Figure 4.21 *Diagram of the experimental setup*

The purpose of the simulation modeling is to verify the maximum rebound height of the sphere relative to the experimental results used to determine the coefficient of restitution. The software tracks the movement of the sphere in XYZ coordinates from the starting point (center of the sphere at a distance of 544.5 mm from the plate, Figure 4.22) to the end point, defined on the top surface of the plate (X = 60 mm, Y = 30 mm, Z = 10 mm).

The maximum rebound height is 167.3 mm, at which the sphere comes to rest (Figures 4.23–4.24). The maximum velocity during motion is 3.19 m/s (Figure 4.25), and the dynamics of the bounces and damping are shown in Figure 4.26.

Figure 4.22 *Initial moment of the simulation.*

Figure 4.23 *Bounce distance at the moment before the sphere changes direction.*

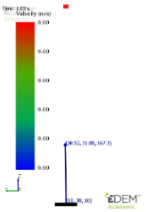

Figure 4.24 *Velocity at the moment before the sphere changes direction.*

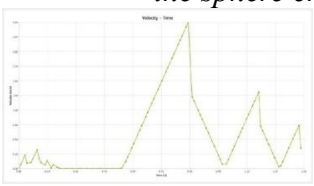

Figure 4.25 *Velocity during free fall of the sphere.*

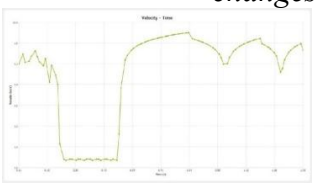

Figure 4.26 *Bounce dynamics during free fall of the sphere.*

The results from the simulation modeling are close to the experimental ones: the average rebound height from the experimental study is h2 = 163,7 mm, and in the simulation it is h2 = 162,8 mm (after correction for the sphere radius of 4.5 mm). The coefficient of restitution experimentally is e = 0.5495, while from the simulation modeling it is e = 0.5490, confirming the validity of the model.

Study of Easy Fil HIPS and TPU materials for 3D printing:

The data obtained from the physical testing are presented in Table 4.9 and Table 4.10, and the data from simulation modeling using EDEM software are presented in Tables 4.11 and 4.12.

Table 4.9 *Coefficient of restitution of EasyFil HIPS with other materials*

Plate/Sphere	Initial height [mm]	D/C	e – Coefficient of restitution SQRT D/C
Easy Fil HIPS (dark)/ Easy Fil HIPS (dark)/	293,36	0,451323	0,279382
Easy Fil HIPS (dark) / TPU	264,8767	0,407503	0,245082
Easy Fil HIPS (dark) / Easy Fil HIPS (blue)	353,2133	0,543405	0,30431
Easy Fil HIPS (dark) / PLA	344,1533	0,529467	0,287751
Easy Fil HIPS (dark) / PETG	338,2267	0,520349	0,255446
Easy Fil HIPS (dark) / Carbon	307,7933	0,473528	0,272056
Easy Fil HIPS (dark) / Steel fill	254,2767	0,391195	0,180176
Easy Fil HIPS (dark) / Vero White	296,92	0,4568	0,225801

Table 4.10 *Coefficient of restitution of TPU material with other materials*

Plate/Sphere	Initial height [mm]	D/C	e – Coefficient of restitution SQRT D/C
TPU / Easy Fil HIPS (dark)	206,7067	0,31801	0,563924
TPU /TPU	197,0167	0,303103	0,550548
TPU / Easy Fil HIPS (blue)	168,72	0,259569	0,509479
TPU /PLA	238,1467	0,366379	0,605293
TPU/PETG	197,1767	0,303349	0,550771
TPU /Carbon	254,1467	0,390995	0,625296
TPU /Steel fill	253,7167	0,390333	0,624767
TPU /Vero White	241,9667	0,372256	0,610128

Table 4.11 *Simulation modeling of the coefficient of restitution with 3D printed material – EasyFil HIPS*

Plate/Sphere	Initial height [mm]	D/C	e – Coefficient of restitution SQRT D/C
Easy Fil HIPS / Easy Fil HIPS (dark)	308,1	0,474	0,688477
Easy Fil HIPS /TPU	262,4	0,403692	0,635368
Easy Fil HIPS / Easy Fil HIPS (blue)	351,1	0,540154	0,734952
Easy Fil HIPS /PLA	352,6	0,542462	0,73652
Easy Fil HIPS /PETG	349,4	0,537538	0,73317
Easy Fil HIPS /Carbon	306,7	0,471846	0,686911
Easy Fil HIPS /Steel fill	256,1	0,394	0,627694
Easy Fil HIPS /Vero White	340	0,523077	0,723241

Table 4.12 *Simulation modeling of the coefficient of restitution with TPU-based 3D printed material*

Plate/Sphere	Initial height [mm]	D/C	e – Coefficient of restitution SQRT D/C
TPU / Easy Fil HIPS (dark)	200,2	0,308	0,554977
TPU /TPU	193,9	0,298308	0,546176
TPU / Easy Fil HIPS (blue)	167,5	0,257692	0,507634
TPU /PLA	245,2	0,377231	0,614191
TPU/PETG	196,3	0,302	0,549545
TPU /Carbon	252,8	0,388923	0,623637
TPU /Steel fill	254,7	0,391846	0,625976
TPU /Vero White	238,4	0,366769	0,605615

Two graphs were created for each type of material to present the results more clearly and comparatively, facilitating comparison with the laboratory experimental data. Figure 4.27 shows a comparative graph of the experimental and simulation data for the EasyFil HIPS material, while Figure 4.28 shows a comparative graph of the experimental and simulation data for the TPU material.

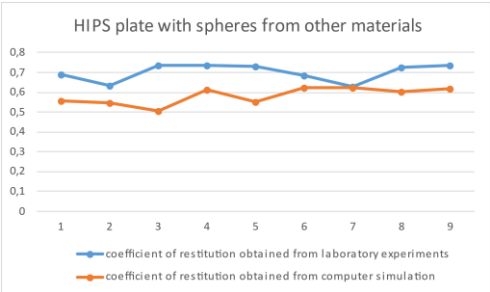

Figure 4.27 *Experimental results for HIPS compared with simulated results;*

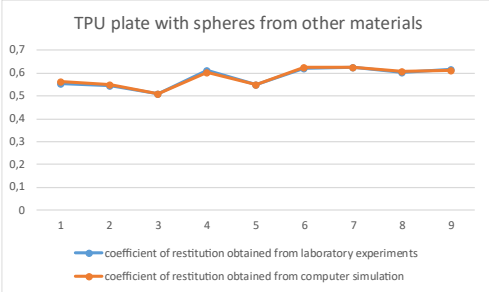

Figure 4.28 *Experimental results for TPU compared with simulated results.*

4.4. Conclusion

Experimental studies on 3D-printed polymer and composite materials showed that sample geometry, process parameters, and material composition have a significant impact on tribological and mechanical properties, including sliding and rolling friction coefficients and the restitution coefficient. Microhardness measurements confirmed the relationship between structural homogeneity and resistance under localized loading, while metallographic observations revealed morphological features and defects important for optimizing 3D printing.

Comparison between experimental data and simulation results showed good agreement (deviations 0.19–7.01%), confirming the validity of the methodology and allowing calibration of models for contact interaction analysis. Special attention was given to Rockwell hardness measurements for soft samples, where correct scale selection and strict adherence to standards ensured reliable results.

UV treatment of resin samples after 3D printing increased surface hardness without affecting the internal structure, with an optimal photopolymerization time of 2–4 minutes for tactile

applications. For flat samples, a minimum thickness of 2–3 mm is required for mechanical strength and to prevent breakage during use.

Chapter 5

Directions for Future Research

Based on the experiments and results obtained, the following directions can be outlined for further research on the tribological and mechanical properties of 3D-printed polymer and composite materials.

5.1. Improvement of 3D Printing Methodologies

Experiments are needed to optimize printing parameters (temperature, layer thickness, orientation) and compare different technologies (FFF, SLA, SLS, PolyJet). The use of recycled and biodegradable materials for sustainable production and new composites with improved properties is promising.

5.2. Expansion of Mechanical and Tribological Studies

Research should include different temperatures, humidity levels, dynamic loading, and surface treatments (UV, plasma, nanocoatings). Micro- and nanoscale measurements (nanoindentation, micro-CT) will enhance understanding of how structure affects material behavior.

5.3. Enhancement of Simulation Models

Development and calibration of DEM/FEM models against experimental data for friction and restitution. Combined simulations enable the creation of digital twins for tribological systems.

5.4. Applications in Engineering and Social Practice

The results support the design of functional and wear-resistant components for industry, medicine, and assistive devices for visually impaired individuals. Creating composites with self-lubricating or self-healing properties is a promising direction.

5.5. Development of Scientific and Applied Knowledge Base

Introducing automated measurement systems and online monitoring will increase experimental accuracy. An expanded database will allow the creation of predictive models and algorithms at the design stage.

5.6. Conclusion

The proposed future steps outline a strategic direction for research that combines experimental, numerical, and applied approaches. Continuing this work will contribute to the development of high-tech solutions in additive manufacturing, optimization of tribological systems, and implementation of smart materials in real engineering applications.

Overall Conclusion

This dissertation presents a systematic study of the tribological and mechanical properties of polymer and composite materials produced using 3D printing technologies. The main objective was to develop, apply, and analyze methodologies for experimental and simulation-based evaluation of material behavior under various loading conditions, examining the relationship between additive manufacturing parameters, sample geometry, and functional performance.

The first chapter provides a literature review and analysis of current advancements in tribology and additive manufacturing, including classification, principles, physical-mechanical dependencies, and factors influencing friction, wear, and restitution.

The second chapter describes the tribological testing technologies, devices, measurement systems, and experimental equipment. Detailed descriptions of apparatus construction, characteristics, and operating principles, along with experimental organization, ensure reproducibility and reliability of results. Main 3D printing technologies and their applications in research and functional material development are analyzed.

Chapter three focuses on the development of research methodologies, including approaches for 3D printing of samples, microhardness analysis, tribological testing (sliding, rolling, restitution coefficients), and simulation using EDEM software. These methodologies form an integrated experimental-analytical system allowing comparison between real and simulated results.

Chapter four presents experimental results and analyses of 3D-printed samples of various materials and geometries, showing clear dependencies between manufacturing parameters, geometry, and mechanical behavior. Optimizing process conditions was shown to improve tribological properties of polymers and composites. Experimental results were compared with simulations, with deviations ranging from 0.19% to 7.01%, confirming the reliability and validity of the proposed models.

Chapter five outlines future research directions, emphasizing improvement of 3D printing methodologies, extrusion parameter optimization, and exploration of new materials, including biodegradable and recycled polymers. Expanding the research database and integrating new analysis technologies will support the creation of more sustainable and functional materials suitable for diverse engineering applications.

In summary, the research advances knowledge in tribology of 3D-printed materials and provides a practical foundation for improving simulation models and experimental methodologies.

SCIENTIFIC AND APPLIED CONTRIBUTIONS

This dissertation makes significant contributions both to the scientific field of tribology of polymer and composite materials and to the practical application of additive manufacturing technologies. The main scientific and applied contributions can be summarized as follows:

1. **Classification of Tribological Processes** – The basic principles, applications, general theories, classical methods, forces, and coefficients in the field of tribology have been analyzed. Based on this analysis, a classification of tribological processes was developed, considering the main principles, applications, general theories, and mechanical, chemical, and physical properties.
2. **Development of Methodologies for Investigating Tribological Properties of 3D-Printed Materials** – Experimental procedures were developed and validated for determining sliding and rolling friction coefficients as well as the restitution coefficient. These methodologies ensure reproducibility and measurement accuracy and can be applied in future studies of new polymers and composites.
3. **Development of Methodologies for Mechanical Properties and Microhardness Analysis** – Using hardness testers (EBP BRV-187.5T) and metallographic observations with Olympus BX53M and digital camera DP23, a precise approach for quantitative determination of material hardness and homogeneity was established. This provides a scientifically grounded basis for evaluating the durability and quality of 3D-printed samples.
4. **Comparison Between Experimental Data and Simulations** – Models developed in EDEM Software allow numerical reproduction of tribological processes and validation of experimental results. Agreements within deviations up to 7% demonstrate the applicability of simulation models for predicting material behavior under contact loading.
5. **Scientific Insights on the Influence of 3D Printing Parameters** – The studies demonstrate the impact of sample geometry, layer thickness, printing orientation, and material composition on tribological and mechanical properties. This knowledge enables optimization of production processes in industrial practice.
6. **Opportunities for Environmentally Sustainable Production** – Approaches for using recycled and biodegradable polymers were developed, laying the foundation for sustainable and eco-oriented production of functional components using additive technologies.
7. **Applied Aspects in Engineering and Social Practice** – The results can be applied in the design of wear-resistant components for mechanical engineering, medical devices, and consumer products, as well as in the development of tactile products for visually impaired individuals, ensuring an optimal balance of hardness, wear resistance, and safety.

In summary, the scientific and applied contribution of this dissertation lies in the creation of an integrated experimental–simulation system for evaluating and optimizing the properties of 3D-printed polymer and composite materials, which finds application both in scientific research and in engineering practice.

REFERENCES

[1] Манолов, Н.Т. и Кандева, М.К., Обща трибология., София Технически университет – София.

[2] Kandeva, M., Vencl, A. and Karastoyanov, D., 2016. Advanced Tribological Coatings for Heavy-Duty Applications: Case Studies. Sofia: Prof. Marin Drinov Academic Publishing House.

[3] Kandeva-Ivanova, M., Karastoyanov, D., Ivanova, B. and Assenova, E., 2016. Tribological Interactions of Spheroidal Graphite Cast Iron Microalloyed with Tin. Sofia: Prof. Marin Drinov Academic Publishing House.

[4] H. P. Jost, "Tribology — Origin and future," Wear, vol. 136, no. 1, pp. 1-17, 1990, doi: 10.1016/0043-1648(90)90068-L

[5] Bultrib, 1963. Tribology in Bulgaria. Beginning and Advance. [online] Available at: https://bultrib.com/?l=1&p=2 [Accessed 5 March 2025]

[6] Bultrib, 2014. 40 Years Tribology in Bulgaria. [pdf] Available at: https://bultrib.com/_data/40_years.pdf [Accessed 5 March 2025]

[7] Assenova, Emilia & Kandeva, M.. (2008). State and outlooks of bulgarian tribology. Journal of the Balkan Tribological Association. 14. 274-283.

[8] Манолов, Н., Кандева, М. и Асенова, Е., 2007. Концепция за развитието на трибологията в България. София: Св. Ив. Рилски.

[9] Държавен вестник, 1990. Брой 34. София: Народно събрание.

[10] ИНГА, 2008. Списание „Контакти". София: Интердисциплинарна гражданска академия.

[11] University of Leeds. (n.d.). Tribology – Functional Surfaces Research. Available at: https://eps.leeds.ac.uk/mechanical-engineering-research-functional-surfaces/doc/tribology?utm_source=chatgpt.com [Accessed 5 March 2025].

[12] Wikipedia. (n.d.). Leibniz Institute of Surface Engineering. Available at: https://en.wikipedia.org/wiki/Leibniz_Institute_of_Surface_Engineering?utm_source=chatgpt.com [Accessed 5 March 2025].

[13] Tokyo University of Science. (n.d.). Initiatives – Tribology Research Center. Available at: https://www.tus.ac.jp/en/initiatives/vol09/?utm_source=chatgpt.com [Accessed 5 March 2025]

[14] Tsinghua University. (n.d.). Tribology Research at Tsinghua University. Available at: https://me.tsinghua.edu.cn/en/info/1248/1840.htm?utm_source=chatgpt.com [Accessed 5 March 2025].

[15] Stachowiak, G.W. & Batchelor, A.W. (2013). Engineering Tribology. 4th ed. Amsterdam: Butterworth-Heinemann.

[16] Kato, K. (2011). Industrial tribology: Trends and challenges for energy-efficient manufacturing. Tribology International, 44(5), pp. 498–508.

[17] Xu, M., Zhang, X., Li, J., & Wang, Y. (2018). Energy loss due to friction and wear in industrial machinery: Global assessment. Energy, 144, pp. 891–902.

[18] Holmberg, K. & Erdemir, A. (2017). The impact of tribology on energy use and CO2 emissions. Tribology International, 115, pp. 1–12.

[19] Jost, H.P. (1966). Lubrication (Tribology) – A Report on the Present Position and Industry Needs. London: Her Majesty's Stationery Office.

[20] Oxford University Press (n.d.). Oxford Dictionary of Science. Available at: https://www.oxfordreference.com

[21] Kotseva, G. & Stoimenov, N. (2025) 'Overview of tribology as an interdisciplinary science', in 19th International Conference on Tribology – SERBIATRIB '25. Kragujevac: Faculty of Engineering, University of Kragujevac. ISBN 978-86-6335-128-8.

[22] American Society for Testing and Materials (ASTM) (2001). ASTM Standards on Wear and Materials Testing. West Conshohocken, PA: ASTM International.

[23] Halling, J. (1979). Principles of Tribology. London: Macmillan.

[24] Organisation for Economic Co-operation and Development (OECD) (1969). Engineering Materials Wear Research Group Report. Paris: OECD.

[25] Rabinowicz, E. (1995). Friction and Wear of Materials. 2nd ed. New York: Wiley.

[26] Тошев, Б. (1973). Теоретична механика. София: Техника.

[27] DoITPoMS (n.d.). Elastic deformation: Hooke's law and stiffness. University of Cambridge. [Available at: https://www.doitpoms.ac.uk/tlplib/mechanical_properties/elastic.php]

[28] LibreTexts (2020). Stress-Strain Curves. LibreTexts Engineering. Available at: https://eng.libretexts.org

[29] Dowling, N.E. (2012). Mechanical Behavior of Materials: Engineering Methods for Deformation, Fracture, and Fatigue. 4th ed. Upper Saddle River, NJ: Pearson.
[30] Barbera, D., Chen, X. & Liu, Y. (2016). Creep-fatigue interaction in materials at high temperature. International Journal of Fatigue, 92(1), pp. 562–573.
[31] Garofalo, F. (1965). Fundamentals of Creep and Creep-Rupture in Metals. New York: Macmillan.
[32] Gellman, A.J. and Spencer, N.D. (2002). Surface chemistry in tribology. Proceedings of the Institution of Mechanical Engineers, Part J: Journal of Engineering Tribology, 216(6), pp. 443–461.
[33] Somorjai, G.A. and Li, Y. (2010). Introduction to Surface Chemistry and Catalysis. 2nd ed. Hoboken, NJ: Wiley-Interscience.
[34] McFadden, C., Soto, C. & Spencer, N. D., 1997. Adsorption and surface chemistry in tribology. Tribology International, 30(12), pp. 881–888
[35] Lenard, J. (2002). Boundary lubrication and tribochemistry.
[36] Hardy, J. and Bircumshaw, H. (1925). The monolayer theory of boundary lubrication.
[37] Merz, R., Brodyanski, R. & Kopnarski, M. (2015). Oxide Film Formation and Tribological Behavior of Stainless Steel Surfaces. Tribology International, 82, pp. 231–242.
[38] Delgado-Brito, I., Hernández-Ramírez, E., Guevara-Morales, G., Figueroa-López, J. & Campos-Silva, J. (2020). Surface Modification of Metals for Tribological Applications: Diffusion and Hardening Processes. Materials Science and Engineering: A, 786, 139398.
[39] Hernández-Ramírez, E., Guevara-Morales, G., Figueroa-López, J. & Campos-Silva, J. (2020). Post-Boriding Diffusion Annealing for Improved Tribological Properties of Steel Components. Surface & Coatings Technology, 385, 125400.
[40] Krishnaraj, R. & Roy, S. (2013). Diffusion Treatments in Tribology: Mechanisms and Applications. Tribology International, 66, pp. 1–12.
[41] Maboudian, R. & Carraro, C. (2004). Surface processes and adhesion in microelectromechanical systems (MEMS). Surface Science Reports, 56(1–4), pp. 1–27.
[42] Pattanaik, S. & Ojha, S. (2021). Tribological Challenges in MEMS Devices and Surface Treatments. Journal of Microelectromechanical Systems, 30(5), pp. 923–936.
[43] Sammoura, F., Hancer, M. & Yang, Y. (2011). Surface Adhesion and Friction in MEMS: Experimental Investigations. Tribology Letters, 44(3), pp. 377–389.
[44] Zhu, X., Chu, J., Chen, W., & Lai, M. (2000). Self-assembled monolayers for MEMS surface modification. Journal of Micromechanics and Microengineering, 10(2), pp. 123–129.
[45] Abdelbary, A. & Chang, L., 2023. Principles of Engineering Tribology: Fundamentals and Applications. eBook. Academic Press. ISBN 9780323991162.
[46] SpecialChem, 2025. Hardness of Plastics - When to Use RockWell & Shore Scales. [online] Available at: https://www.specialchem.com/plastics/guide/hardness-introduction [Accessed: 20 April 2025].
[47] EBPU Electromechanical Equipment (Zhejiang) Co. Ltd. (n.d.) Digital Universal Hardness Tester BRV-187.5T Testing Machine With Close Loop Load Cell [online]. Available at: https://www.hardnesstesting-machine.com/Digital-Universal-Hardness-Tester-BRV-187-5T-Testing-Machine-With-Close-Loop-Load-Cell-pd49740224.html (Accessed: 2 May 2025).
[48] NAC Memrecam https://www.nacinc.com/ (last accessed Sep. 2025)
[49] Stoimenov N., Kotseva G., Georgieva V., Classification of 3D print technologies, 34th International Scientific and Technical Conference Automation of Discrete Production Engineering 2025, ISBN 978-619-7667-74-5, DOI: 10.53656/adpe-2025, Publisher: Az-buki National Publishing House, pp. 40-53
[50] Kotseva G., Stoimenov N., Klochkov L.. Tribological Studies of 3D Printed Filaments. An Overview. XXXII International Scientific and Technical Conference, ADP - 2023., Sozopol, Bulgaria, Publishing house of TU-Sofia Publisher Department “Automation of Discrete Production Engineering“, 2023, ISSN:2682-9584, 150-154
[51] Acierno, D., 2023. Fused Deposition Modelling (FDM) of Thermoplastic Materials. Available at: https://pmc.ncbi.nlm.nih.gov/articles/PMC10744784/ [Accessed 5 May 2025].
[52] Stratasys, 2025. Stereolithography (SLA) 3D Printing Technology. [online] Available at: https://www.stratasys.com/en/guide-to-3d-printing/technologies-and-materials/stereolithography-technology/?utm_source=chatgpt.com [Accessed 2 May 2025].
[53] Formlabs, 2025. Ultimate Guide to Stereolithography (SLA) 3D Printing. [online] Available at: https://formlabs.com/blog/ultimate-guide-to-stereolithography-sla-3d-

printing/?srsltid=AfmBOoo0UY6N5mVIa26XASmWg3tPARJpyhzQOtKiykFjisSlpayTB96T&utm_source=chatgpt.com [Accessed 2 May 2025].
[54] Berman, B., 2012. 3-D printing: The new industrial revolution. Business Horizons, 55(2), pp.155–162.
[55] Melchels, F.P.W., Domingos, M.A.N., Klein, T.J., Malda, J., Bartolo, P.J. & Hutmacher, D.W., 2010. Additive manufacturing of tissues and organs. Progress in Polymer Science, 37(8), pp.1079–1104.
[56] Jackson Sanders, Xingjian Wei, Zhijian Pei, Experimental Investigation of PolyJet 3D printing: Effects of Sample Location and Volume on Power Consumption, Manufacturing Letters, Volume 31, 2022, Pages 83-86, ISSN 2213-8463, https://doi.org/10.1016/j.mfglet.2021.07.013. https://www.sciencedirect.com/science/article/pii/S2213846321000584
[57] Sinterit, 2025. Selective Laser Sintering in Details. [online] Available at: https://sinterit.com/blog/sls-technology/selective-laser-sintering-in-details/?utm_source=chatgpt.com [Accessed 5 July 2025].
[58] 3DS, 2025. SLS – Selective Laser Sintering. [online] Available at: https://www.3ds.com/make/service/3d-printing-service/sls-selective-laser-sintering?utm_source=chatgpt.com [Accessed 5 July 2025].
[59] Herzog, D., Seyda, V., Wycisk, E. & Emmelmann, C., 2016. Additive manufacturing of metals. Acta Materialia, 117, pp.371–392.
[60] Gibson, I., Rosen, D.W. & Stucker, B., 2021. Additive Manufacturing Technologies: 3D Printing, Rapid Prototyping, and Direct Digital Manufacturing. 3rd ed. Springer, Cham.
[61] Sachs, E., Cima, M., Williams, P., Brancazio, D. & Cornie, J., 1992. Three-dimensional printing: Rapid tooling and prototypes directly from a CAD model. Journal of Engineering for Industry, 114(4), pp.481–488.
[62] Huang, S.H., Liu, P., Mokasdar, A. & Hou, L., 2013. Additive manufacturing and its societal impact: a literature review. International Journal of Advanced Manufacturing Technology, 67, pp.1191–1203.
[63] Derby, B., 2010. Inkjet printing of functional and structural materials: fluid property requirements, feature stability, and resolution. Annual Review of Materials Research, 40, pp.395–414.
[64] Klosterman, D. A. (1999) Accuracy Study on Laminated Object Manufacturing for the Metallic … [pdf] University of Texas at Austin. Available at: https://utw10945.utweb.utexas.edu/Manuscripts/1999/1999-082-Suping.pdf (Accessed: 1 June 2025).
[65] Stratasys (2015) "Objet260 Connex 1-2-3 3D Printers", Support Center, 2015. Available at: https://support.stratasys.com/en/Printers/PolyJet-Legacy/Objet260-Connex-1-2-3 (Accessed: 8 June 2025).
[66] Sabor SRL. (2015). Objet260 Connex3 – Specification Sheet. [online] Available at: https://www.sabor-srl.com/wp-content/uploads/2017/05/Objet260-Connex3-Spec-Sheet-English-Web-08-2015.pdf [Accessed 15 July 2025].
[67] Stratasys. (n.d.). Objet260 Connex 1/2/3 – Support Portal. [online] Available at: https://support.stratasys.com/en/printers/polyjet-legacy/objet260-connex-1-2-3 [Accessed 15 July 2025].
[68] Ellsworth Adhesives. (n.d.). Objet260 Connex3 3D Printer Product Page. [online] Available at: https://www.ellsworth.co.th/product/product_100003108157912.html [Accessed 15 July 2025].
[69] Applicad Indonesia. (n.d.). Objet260 Connex3 – Stratasys Design Series. [online] Available at: https://www.applicadindonesia.com/3d-printer/stratasys-design-series/objet260-connex3/ [Accessed 15 July 2025].
[70] Proto3000. (n.d.). Objet260 Connex3 3D Printer. [online] Available at: https://proto3000.com/product/objet260-connex3/ [Accessed 15 July 2025].
[71] Anycubic (2024) Photon M3 Max – Specifications. Available at: https://www.anycubic.com/products/photon-m3-max [Accessed: 21 July 2025].
[72] Chockalingam, K. & Jawahar, N. (2017) A review of stereolithography process and its applications in additive manufacturing, Materials Today: Proceedings, 4(2), pp. 1140–1150. DOI: 10.1016/j.matpr.2017.01.133.
[73] Hull, C. W. (1986) Apparatus for production of three-dimensional objects by stereolithography, U.S. Patent 4,575,330.
[74] Gibson, I., Rosen, D. W. & Stucker, B. (2020) Additive Manufacturing Technologies: 3D Printing, Rapid Prototyping, and Direct Digital Manufacturing, 3rd edn., Springer, Cham.
[75] TWI Global (n.d.) What is Stereolithography (SLA)? Available at: https://www.twi-global.com/technical-knowledge/faqs/what-is-stereolithography [Accessed: 21 July 2025]
[76] Fouly, A., Assaifan, A.K., Alnaser, I.A., Hussein, O.A. & Abdo, H.S., 2022. Evaluating the Mechanical and Tribological Properties of 3D Printed Polylactic-Acid (PLA) Green-Composite for Artificial Implant: Hip Joint Case Study. Polymers, 14(23), p.5299.
[77] Santo, J., Ali, H., Kumar, V. & Zhang, Y., 2024. Effect of composite processing technique on tribological behavior of 3D-printed PLA/graphene composites. Wear, [online] Available at: https://www.sciencedirect.com/science/article/abs/pii/S0301679X24006479.

[78] Wang, C., Li, Z., Chen, H. & Liu, J., 2024. Mechanical and tribological performance of FDM printed polymer composites: Influence of process parameters. Wear, [online] Available at: https://www.sciencedirect.com/science/article/abs/pii/S0301679X23009891.

[79] Formlabs (n.d.) Guide to 3D Printing Materials: Types, Applications, and Properties [online]. Available at: https://formlabs.com/blog/3d-printing-materials/ (Accessed: June 2025).

[80] Стоименов Н., Карастоянов Д., Изследване движението и взаимодействието на различни форми мелещи тела., XXIV МНТК Автоматизация на дискретното производство „АДП – 2015" 18-21 Юни, Созопол 2015г., стр.148-153, ISSN – 13 10 -3946.

[81] Stoimenov N., Ruzic J., INVESTIGATION OF MILLING PROCESSES IN HIGH ENERGY MILL (ATTRITOR)., XXV International Scientific and Technical Conference, ADP -2016., June 23-26th 2016, Sozopol, Bulgaria., pp.85-90, ISSN – 13 10 -3946.

[82] Stoimenov N., Investigation of iron ore material for milling in semi-autonomous ball mill with standard lifter shape., XXVI International Scientific and Technical Conference, ADP - 2017., June 22-25th 2017, Sozopol, Bulgaria., pp. 61-65, ISSN – 13 10 -3946.

[83] Stoimenov N., Sabotinkov N., Popov B., Investigation of Materials Behavior in Autogenous Grinding Mill, 8th International Conference on Mechanical Technologies and Structural Materials (MTSM 2018), Split, Croatia, September 27-28, 2018, Croatian Society for Mechanical Technologies, Croatia, ISSN: 1847-7917, pp. 173-176

[84] N. Stoimenov, J. Ruzic, Analysis of the particle motion during mechanical alloying using EDEM software, 19th IFAC Conference on Technology, Culture and International Stability, TECIS 2019, Volume 52, Issue 25, November 2019, IFAC-PapersOnLine, Publisher: IFAC Secretariat, ISSN:2405-8963, pp 462-466

[85] Stoimenov N., Panev P., Karastoyanov D., Software for 3D Modeling, Simulation and Optimization, XXVII International Scientific and Technical Conference, ADP - 2018., June 21-24th 2018, Sozopol, Bulgaria., pp. 329-334, ISSN – 13 10 -3946.

[86] Kotseva, G., Stoimenov, N., Gyoshev, S., Georgieva, V.. Tribological Processes in TPU and HIPS 3D Printing Materials. 18th International Conference on Control, Automation, Robotics and Vision (ICARCV 2024), Published by IEEE, 2025, 1136-1141

[87] M. P. F. Dunne, A. A. A. Alshahrani, J. A. E. Wriggers, Prediction of wear in polymer materials: A review, Wear, 426-427, pp. 226-241, 2019.

[88] N. Ayrilmis, M. Kariz, J.H. Kwon, M. Kitek Kuzman, Effect of printing layer thickness on water absorption and mechanical properties of 3D-printed wood/PLA composite materials, Int. J. Adv. Manuf. Technol., 102 (5-8), pp. 2195-2200, 2019.

[89] Kotseva G., Stoimenov N., Kandeva M.. Tribological processes in the material for 3D printing filament HIPS. 12th International Conference on Mechanical Technologies and Structural Materials (MTSM 2023), Croatian Society for Mechanical Technologies, Croatia, 2023, ISSN:1847-7917, 137-144

[90] https://www.tianxing.com.cn/uploadfile/202101/b3a46b115c.pdf [Last accessed May, 2025]

[91] Kotseva G., Georgieva V., Gyoshev S.. Investigation of Tribological Parameters of 3D Printed Samples. International Scientific Journal Machines.Technologies.Materials, 19, 8, Scientific and technical union of mechanical engineering, 2023, ISSN:ISSN (Print) - 2535-0153 ISSN (Online) - 2535-0161, 255-259

[92] Stoimenov N., Arsova M., Tomova M., Kotseva G., Kandeva M.. Investigation of tactile suitability in contact with 3D printed PLA material with visually impaired people. Journal of the Balkan Tribological Association, 4, 29, Scientific Bulgarian Communications, 2023, ISSN:1310-4772, 581-590. SJR (Scopus):0.21

[93] Софийски университет "Св. Климент Охридски" (2024) „Залите и пространствата във ФНОИ са напълно обозначени с брайлови табели", Новини и събития, 30 април 2024 г. [онлайн]. Достъпно на: https://www.uni-sofia.bg/index.php/novini/novini_i_s_bitiya/zalite_i_prostranstvata_v_v_fnoi_sa_nap_lno_oboznacheni_s_brajlovi_tabeli (Достъп: юни 2025 г.).

[94] Stoimenov, N., Gyoshev, S. & Kotseva, G., 2025. A Study of the Hardness of 3D-Printed Materials for Blind Applications. 3rd International Conference on Computers in Natural Sciences, Biomedicine and Engineering (COMCONF), accepted for publication